

Journal Pre-proofs

Novel Benzimidazole-Triazole Hybrids as Apoptosis Inducing Agents in Lung Cancer: Design, Synthesis, ^{18}F -Radiolabeling & Galectin-1 Inhibition Studies

Nerella Sridhar Goud, Venkatesh Pooladanda, K. Muni Chandra, P.S. Lakshmi Soukya, Ravi Alvala, Pardeep Kumar, Chandana Nagraj, Rose Dawn Bharath, Insaf A. Qureshi, Chandraiah Godugu, Mallika Alvala

PII: S0045-2068(20)31422-X
DOI: <https://doi.org/10.1016/j.bioorg.2020.104125>
Reference: YBIOO 104125

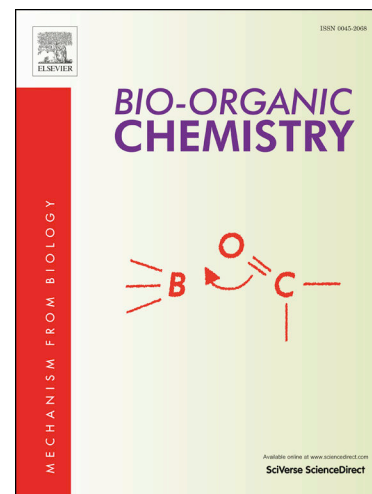
To appear in: *Bioorganic Chemistry*

Received Date: 2 June 2020
Accepted Date: 19 July 2020

Please cite this article as: N. Sridhar Goud, V. Pooladanda, K. Muni Chandra, P.S. Lakshmi Soukya, R. Alvala, P. Kumar, C. Nagraj, R. Dawn Bharath, I.A. Qureshi, C. Godugu, M. Alvala, Novel Benzimidazole-Triazole Hybrids as Apoptosis Inducing Agents in Lung Cancer: Design, Synthesis, ^{18}F -Radiolabeling & Galectin-1 Inhibition Studies, *Bioorganic Chemistry* (2020), doi: <https://doi.org/10.1016/j.bioorg.2020.104125>

This is a PDF file of an article that has undergone enhancements after acceptance, such as the addition of a cover page and metadata, and formatting for readability, but it is not yet the definitive version of record. This version will undergo additional copyediting, typesetting and review before it is published in its final form, but we are providing this version to give early visibility of the article. Please note that, during the production process, errors may be discovered which could affect the content, and all legal disclaimers that apply to the journal pertain.

© 2020 Published by Elsevier Inc.



Novel Benzimidazole-Triazole Hybrids as Apoptosis Inducing Agents in Lung Cancer: Design, Synthesis, ¹⁸F-Radiolabeling & Galectin-1 Inhibition Studies.

Nerella Sridhar Goud ^{a,b}, Venkatesh Pooladanda ^c, Muni Chandra K ^a, P.S. Lakshmi Soukya ^a, Ravi Alvala ^d, Pardeep Kumar ^b, Chandana Nagraj ^b, Rose Dawn Bharath ^b, Insaf A. Qureshi ^e, Chandraiah Godugu ^c, Mallika Alvala ^{a*}

^a Department of Medicinal Chemistry, National Institute of Pharmaceutical Education and Research (NIPER), Hyderabad 500 03 7, India

^b Department of Neuroimaging and Interventional Radiology (NI & IR), National Institute of Mental Health and Neuro Sciences (NIMHANS), Bangalore 560 029, India.

^c Department of Regulatory Toxicology, National Institute of Pharmaceutical Education and Research (NIPER), Hyderabad 500 037, India

^d G. Pulla reddy College of Pharmacy (GPRCP), Hyderabad 500 028, India

^e Department of Biotechnology & Bioinformatics, School of Life Sciences, University of Hyderabad (UOH), Hyderabad-500046, India.

*Corresponding Address:

Dr. Mallika Alvala, PhD
Department of Medicinal Chemistry
NIPER-Hyderabad
Email: mallikaalvala@yahoo.in

Abstract

In this study, we have synthesized a new series of benzimidazole-triazole hybrids as galectin-1 (gal-1) mediated apoptosis-inducing agents, and evaluated for their potential anticancer activity against a panel of human cancer cell lines *viz.* breast cancer (MCF-7 and MDA-MB-231) lung cancer (A-549 and NCI-H460), and human keratinocyte cancer (HaCaT), using MTT assay. The target compound **7c** exhibited an excellent growth inhibition against lung cancer (A-549 and NCI-H460) cells with an IC₅₀ value of 0.63±0.21 μM, and 0.99±0.01 μM respectively. The target compound **7c** also showed a significant growth inhibition against breast cancer (MCF-7 and MDA-MB-23) with an IC₅₀ value of 1.3±0.18 μM, and 0.94±0.02 μM respectively. In addition, the radiochemical synthesis has been performed using fluorine-18 radionuclide in the GE Tracer-lab FX2N module to prove the target compound **7c** as a PET imaging agent. In the final stage, the ¹⁸F-**7c** target compound was successfully purified with 60% ethanol in water. The radiochemical purity was achieved > 95 % using HPLC, and the residual solvent DMF limit was around 78 ± 3 ppm confirmed by GC analysis. Further, the apoptosis induction by **7c** in lung cancer (A-549) cells was confirmed as a result of the decrease in MMP levels, increased percentage of apoptotic cells, and sub G1 phase arrest by JC-1 staining, DAPI staining, annexin V-FITC/PI, and flow cytometric analysis. In addition, the target compound **7c** significantly reduced the gal-1 protein levels in a dose-dependent manner as confirmed by ELISA studies. The protein binding studies like Surface Plasmon Resonance (SPR) and Fluorescence Spectroscopy (FS) studies indicated that the target compound **7c** is capable of binding to gal-1 with an equilibrium constant (K_D) value of 1.19E-06 M, and binding constant (K_a) of 9.5 x 10³ M⁻¹ respectively. The *in-silico* computational studies also revealed possible interactions and pharmacokinetic properties (ADMET) of compound **7c** with the binding domain of gal-1. Therefore, the novel benzimidazole-triazole hybrids as apoptosis-inducing agents in lung cancer would be potential cytotoxic and PET imaging agents *via* gal-1.

Key Words: benzimidazole-triazole, galectin-1, apoptosis, fluorine-18, positron emission tomography.

Research Highlights

- The **7c** is a potent cytotoxic agent against global major leading lung cancer burden.
- It has shown IC_{50} of $0.63\pm 0.21 \mu\text{M}$, and $0.99\pm 0.01 \mu\text{M}$ in lung cancer cells (A-549 and NCI-H460) mediated by gal-1.
- The **7c** is capable of binding with gal-1 based on the confirmation studies of SPR, and FS.
- The ^{18}F -**7c** radiotracer is considered as an ideal PET tracer due to its 110 min half-life.
- The radiochemical purity & identity of ^{18}F -**7c** was validated as per cGMP guidelines for clinical evaluation.

1. Introduction

Cancer is the second major dreadful disease globally and, around 1 in 6 persons are being diagnosed with cancer as per recent reports of the World Health Organization (WHO). Globocan 2018 reported that the top three high frequent cancer types mainly lung, female breast, and colorectal cancer, which are responsible for one-third of the cancer incidence and mortality burden worldwide [1, 2]. The most commonly diagnosed cancer case is lung cancer with the highest ratio of 11.6 % new cases and 18.4 % death cases followed by female breast, and colorectal cancer globally. Lung cancer accelerated over the decades from 3 % during 2008-09 to 11% 2019-20 [3]. Hence, it is necessary to develop highly effective and selective chemotherapeutic agents for lung cancer treatment.

Galectin-1(gal-1), 14KDa protein belongs to galectin group of lectin family. It affects cellular processes like extracellular & intracellular signaling pathways *via* protein-protein interactions with other cytoplasmic, and nuclear proteins through specific binding to cell-surface, and extracellular matrix glycans [4]. A wide variety of gal-1 biological phenomena has been reported such as cell adhesion, proliferation, apoptosis, T cell receptor counter-stimulation, immunomodulatory effects, cell cycle arrest, pre-B cell signaling, RNA splicing, and promotion of H-Ras membrane anchorage *etc.* [5, 6]. Among the 15 mammalian galectins, gal-1 is the first discovered protein in the family which is expressed ubiquitously in the mammalian organism. It has been reported to overexpress/upregulated in many tumor types including lung, astrocytoma, melanoma, prostate, thyroid, colon, bladder, and ovary carcinomas [7, 8]. Gal-1 is regarded as a biomarker in various events like diagnosis, prognosis and treatment condition of different tumor types [9]. *Wei-an chang et al*, reported the role of

galectins mainly gal-1 in lung cancer and indicated that gal-1 is highly expressed in invasive lung cancer cells and leads to promote lung cancer cell migration and invasion [10]. Therefore, the development of novel anticancer agents *via* targeting gal-1 protein would be a fruitful strategy in lung cancer treatment.

The Positron Emission Tomography (PET) is regarded as a remarkable molecular imaging modality to study the pathophysiology, and pharmacological conditions in the animals, human subjects, and to evaluating drug development [11]. The PET modality plays a wide role in medical diagnosis, mainly in oncology, psychiatry and neurology. The major advantage of PET is to measure very low concentration of radiotracers at a specific region of interest in a living subject, either animal or human or, throughout a whole body [12]. Therefore, it is essential to focus on radiochemical synthesis and its quality control studies to achieve good PET imaging agents for early diagnosis. Nevertheless, the availability of ^{11}C , ^{13}N , ^{15}O , the ^{18}F isotope is widely used radionuclide in the radiolabelling of various bioactive molecules for PET imaging due to its positron-emitting property and suitable half-life of 110 min [13]. In clinical practice, the ^{18}F -FDG (Fluorodeoxyglucose-FDG) is being used routinely in the diagnosis of different tumor types & neurological diseases using PET modality [14]. The clinically available anticancer drugs like doxorubicin, paclitaxel, erlotinib, and gefitinib are also being used as PET imaging agents in human subjects, which are successfully labeled with ^{18}F radionuclide or technetium-99m *etc.* These drugs are capable to exhibit their potential side effects when used as cytotoxic agents due to high concentration, but still being used as PET tracers without major side effects due to nanomole concentration range for PET diagnosis [15-18]. Here, our goal is to prove the feasibility of the radiochemical synthesis of the target molecule in addition to its chemical synthesis, computational studies, and *in-vitro* biological evaluation. Further to develop this ^{18}F -7c tracer as a real PET imaging agent for clinical use, the preclinical, toxicity and tracer distribution studies need to be assessed.

Benzimidazole is a fused heterocyclic ring system consisting of benzene, and imidazole rings, it forms an integral part of vitamin B12 [19]. It is known for its crucial role in numerous diseases like cancer, microbial infection, tuberculosis, Alzheimer's *etc.* through various mechanisms like apoptosis, microtubulin inhibition, DNA intercalation, protein kinase inhibition, aromatase inhibition, and HSP90 inhibition [20-21]. Some USFDA approved drugs contain benzimidazole nucleus are already well established and successfully used in the treatment of multiple diseases [22]. The substitution pattern of benzimidazole is essential

for selectivity, and it is reported that the N-1, C-2, C-5, and C-6 positions are widely explored for anticancer potentials [23-24]. *Tsung-Chieh Shih et al.* reported a novel gal-1 inhibitor LLS30 (**I**), it has exhibited synergistic anti-cancer activity with docetaxel, and also potentially inhibited the invasion and metastasis of prostate cancer *in vivo* [25]. The same group had also reported another novel gal-1 inhibitor LLS2 (**II**), it was reported to potentiate the anticancer potentials of Paclitaxel *in vivo* [26]. Recently, our research group reported 1-benzyl-1H-benzimidazole derivatives as gal-1 mediated anticancer agents, and the target compound (**III**) had shown a significant growth inhibition against breast cancer (MCF-7) cells with an IC_{50} value of $7.01 \pm 0.20 \mu\text{M}$. The binding affinity of target compound with gal-1 was confirmed by Fluorescence Spectroscopy (FS), and Surface Plasmon Resonance (SPR) with their respective inhibition (K_D and K_i) values [27]. A new series of morpholines linked coumarin-triazole hybrids have been reported as potential anticancer agents *via* gal-1 inhibition, and the target compound (**IV**) exhibited a significant growth inhibition against bone cancer (MG-63) cells with an IC_{50} of $0.80 \pm 0.22 \mu\text{M}$. The FS, and SPR studies confirmed the binding of target compound to gal-1 [28] (**Fig. 1**).

<insert Figure 1 here>

The role of gal-1 in various stages of tumor development, and the importance of PET modality for early diagnosis have triggered our interest to develop highly selective target-specific anticancer agents. Hence, the current study mainly focused on novel benzimidazole-triazole hybrids as apoptosis-inducing agents in lung cancer, their design, synthesis, ^{18}F -radiolabeling & galectin-1 inhibition studies.

2. Results and discussion

2.1. Chemistry

The target benzimidazole-triazole hybrids (**7a-t**) were synthesized by utilizing Huisgen 1,3-dipolar cycloaddition reaction of terminal alkyne of benzimidazole intermediate (**6**) with various benzyl (or) phenyl azides in the presence of copper(I)-catalyst (**Scheme 1**) [29]. Initially, the N-benzyl-4-chloro-2-nitroaniline (**3**) was synthesized through a green approach using 4-chloro-2-nitro aniline with benzyl bromide. Further, the compound (**3**) was reduced with stannous chloride dehydrate offered N1-benzyl-4-chlorobenzene-1,2-diamine (**4**) [30]. In the next step, the 4-hydroxy benzaldehyde was reacted with N1-benzyl-4-chlorobenzene-1,2-diamine (**4**) using ethanol in the presence of sodium metabisulphite furnished 4-(1-benzyl-6-chloro-1H-benzo[d]imidazol-2-yl) phenol intermediate (**5**) [31], it had further

offered 1-benzyl-6-chloro-2-(4-(prop-2-yn-1-yloxy) phenyl)-1H-benzo[d]imidazole (**6**) upon treatment with propargyl bromide in the presence of potassium bromide using acetone. Finally, the 1,3-dipolar cycloaddition of benzimidazole intermediate (**6**) with various benzyl (or) phenyl azides furnishing target compounds **7a-t** with moderate to good yields.

<Insert scheme 1 here>

All synthesized compounds (**7a-t**) were characterized by spectral techniques *viz.* ¹H-NMR, ¹³C NMR and HRMS. The ¹H NMR spectrum of **7a** showed characteristic protons of O- and N-attached methylene groups at δ 5.60 and 5.33 ppm respectively. All the remaining protons appeared in the range of δ 7.00-8.98 ppm. ¹³C NMR spectrum showed the characteristic O- and N-attached methylene carbons at δ 61.63 and δ 48.23 ppm respectively, and all the remaining carbons appeared in the range of δ 112.95-159.86. A similar pattern was observed for the rest of the compounds (**7a-t**).

2.2. Radiochemistry

The radiochemical synthesis is an essential task, and it shows a major impact on the quality of PET images for the diagnosis, and the quality control studies like colour appearance, pH, purity, residual solvents, stability and, sterility *etc.* must be passed as per the limitations of the Food Drug Administration (FDA) Q3C(R6) and Current Good Manufacturing Practice (cGMP) guidelines for clinical use. *Dolle et al*, have reported different methods and reaction conditions of ¹⁸F labeled fluoropyridines through aromatic and, heteroaromatic nucleophilic substitution mechanism, and reported the favourable conditions like an activated Kriptofix K[¹⁸F] F-K222 complex and aprotic solvent like Dimethyl Sulfoxide (DMSO) with the no-carrier-added, at high temperature around 120-150 °C for 2-3 minutes for ¹⁸F radiolabeling of pyridine by replacing chlorine atom at C-2 position, and offered high radiochemical yields [32].

Here, we adopted the above method of radiochemical synthesis for ¹⁸F radiolabeling of the target molecule **7c** with a chloro substitution at the C-6 position through the aromatic nucleophilic substitution mechanism, and succeeded with high radiochemical purity and good yields. Initially, the [¹⁸F] radionuclide was generated through ¹⁸O (p, n)¹⁸F nuclear reaction in the cyclotron. The radiochemical synthesis was carried out in the GE tracer lab FX2N synthesis module using 350 ± 20 mCi of ¹⁸F radionuclide from the cyclotron. In the hot cell, the reaction was started with trapping of ¹⁸F radionuclide in the Quaternary

Ammonium Anion exchange (QMA) cartridge and further, it was eluted by kryptofix (K222) solution through QMA into the reactor vial (**Fig. 2**). The activated Kryptofix K[¹⁸F] F-K222 complex was dried at a high temperature of 90 °C for 10 minutes. Finally, the radiolabeling of ¹⁸F-7c was carried out by reacting the precursor molecule (**7c**) in Dimethylformamide (DMF) with dried Kryptofix K[¹⁸F] F-K222 complex (**Scheme-2**) [33].

<Insert Figure 2 here>

<Insert scheme 2 here>

After completion of synthesis, the purification was achieved by washing the reaction mixture with purified water followed by treatment with 20%, and 40% ethanol, and the maximum elution was achieved with 60% ethanol solution. The radiochemical purity was confirmed by the High-Pressure Liquid Chromatography (HPLC) analytical method, and the traces of free ¹⁸F radionuclide always appears at low retention time, and the target compound ¹⁸F-7c appeared at 9.830 min using radio detector (**Fig. 3A**), whereas the cold target compound retention time was found to be 9.267 min by HPLC method using Uv detector (**Fig. 3B**). Thus, almost equal retention time of ¹⁸F-7c with its cold target compound validated the ¹⁸F radiolabeling with the precursor molecule (**7c**), and proven it was our radiolabeled molecule of interest ¹⁸F-7c. The yield of the ¹⁸F-7c was around 6 ± 1% after purification through HLB cartridge, and the radiochemical purity was achieved > 95 % by HPLC method. The stability studies were also performed post synthesis 1 hr, 2 hr, and found that there were no additional metabolite peaks of the final product ¹⁸F-7c on the HPLC chromatogram indicated that the ¹⁸F-7c is metabolically stable. The Dimethylformamide (DMF) residual solvent levels were found to be 78 ± 3 ppm in the final formulation using Gas Chromatography (GC) analysis (**Fig. 4**), the DMF levels were within the acceptable limits as per the guidelines of Food Drug Administration (FDA) Q3C(R6) because the DMF is a class-II solvent, and the recommended limit is 880 ppm. The ethanol residual solvent was found to be in higher ppm concentration in GC analysis since it was an eluting solution. The European Medicines Agency (EMA), and United States Food and Drug Administration (USFDA) had found a greater ppm concentration of ethanol in the final formulation of many radiopharmaceuticals, it might be considerable as which are synthesized, and radiolabeled in cGMP conditions and the final radiopharmaceutical formulations are further diluted with saline or water to reduce the radioactive concentration [34]. Therefore, our study successfully proved the radiolabeling of synthesized **7c** with ¹⁸F radionuclide, and the final radiolabeled ¹⁸F-7c

would be a potential PET imaging against upregulated gal-1 protein in lung cancer through validating further confirmation studies like preclinical, toxicity and tracer distribution studies.

<Insert Figure 3A & 3B here>

<Insert Figure 4 here>

2.3. Biological evaluation

2.3.1. *In vitro* cytotoxic activity

The synthesized benzimidazole-triazole derivatives (**7a-t**) were screened for their *in vitro* cytotoxicity against a panel of human cancer cell lines *viz.* breast cancer (MCF-7 and MDA-MB-231) lung cancer (A-549 and NCI-H460), and Human keratinocyte cancer (HaCaT), using 3-(4,5-dimethylthiazol-2-yl)-2,5-diphenyltetrazolium bromide (MTT) assay [35]. The IC₅₀ (μM) values of synthesized compounds (**7a-t**) and the standard, 5-fluorouracil are displayed in **Table-1**. Among all, the compound **7c** had shown significant growth inhibition with an IC₅₀ of 1.3±0.18μM, 0.99±0.01 μM, 0.94±0.02 μM, 0.63±0.21μM, 2.99±0.09 μM against MCF-7, NCI-H460, MDA-MB-231, A-549, and HaCaT cell lines respectively with 8.43% inhibition on normal Rattus Norvegicus Kidney (NRK) cells. Further mechanistic studies of **7c** were carried in A-549 cell line at different concentrations based on its potency towards lung cancer cell lines.

The Structural activity relationship (**SAR**) revealed that all synthesized compounds had shown excellent to good activity in all selected cancer cell lines. The compounds namely **7b**, **7c**, **7f**, **7g**, **7i** and **7n** exhibited prominent growth inhibition against breast cancer (MCF-7 and MDA-MB-231) lung cancer (A-549 and NCI-H460), and Human keratinocyte cancer (HaCaT) in the range of 0.63-8.58 μM. The target compound **7c** with 3-hydroxy phenyl substitution exhibited an excellent growth inhibition against lung cancer (A-549 and NCI-H460) cells with an IC₅₀ value of 0.63±0.21 μM, and 0.99±0.01 μM respectively. It also showed a significant growth inhibition against breast cancer (MCF-7 and MDA-MB-23) with an IC₅₀ value of 1.3±0.18 μM, and 0.94±0.02 μM respectively. The compound **7g** with 3-fluoro substitution exhibited good cytotoxicity against lung cancer (A-549) cells with an IC₅₀ value of 1.11±0.12 μM, whereas, another potent compound **7n** with 4-nitro substitution had shown good cytotoxicity against lung cancer (NCI-H460) and Human keratinocyte cancer (HaCaT) cells with an IC₅₀ value of 1.98±0.08 μM and 1.35±0.09 μM respectively. The compound **7f** with 4-fluoro substitution had shown good cytotoxicity against breast

cancer (MCF-7) cells with an IC_{50} value of $1.21 \pm 0.17 \mu\text{M}$. The compound **7i** with 4-nitro-2-chloro substitution exhibited good cytotoxicity against breast cancer (MDA-MB-23) cells with an IC_{50} value of $1.65 \pm 0.05 \mu\text{M}$. The rest compounds have shown less cytotoxicity against selected cell lines. Over all, compound **7c** was proved to be the best cytotoxic agent among all.

<Insert Table 1 here>

2.3.2. Observations of morphological changes using phase contrast microscopy

The distinct features of programmed cell death or apoptosis are recognized by the changes in the molecular, biochemical and morphology of a cell [36]. The cells (A-549) treated with compound **7c** at different concentrations of 0.5, 1 and $2.5 \mu\text{M}$ showed promising morphological changes such as formation of membrane blebs, and cell shrinkage with cells rounding as evidenced by phase contrast microscopy studies and corresponding to the concentration (**Fig. 5**). However, there are no distinctive features of morphological changes found in the controlled cells.

<Insert Figure 5 here>

2.3.3. DAPI nucleic acid staining

This study distinguishes normal cells from apoptotic cells by staining the condensed nuclei of apoptotic cells using DAPI (4',6-diamidino-2-phenylindole), a blue fluorescent dye assists in the visualization of nuclear damage or chromatin condensation of apoptotic cells, which are of high interest to detect the apoptosis induction by compound **7c** in lung cancer (A-549) cells [37]. The results from **Fig. 6** clearly suggested that the treated cells with compound **7c** at different concentrations of 0.5, 1 and $2.5 \mu\text{M}$ showed condensed, fragmented or horse-shoe shaped nuclei in the cells, whereas the nuclear structure of controlled cells was intact.

<Insert Figure 6 here>

2.3.4. Cell cycle analysis

Damage of DNA content is an essential feature of apoptosis. The changes in the frequency of treated cells with compound **7c** in every phase have been observed corresponding to control cells. A-549 cells were treated with compound **7c**, at different concentrations of 0.25, 1 and $2.5 \mu\text{M}$ for 24 h, followed by stained with Propidium Iodide (PI), and cell death was quantified by using BD FACSVerse™ flow analyser [38]. The PI staining of treated cells with **7c** at different concentrations exhibited an increase in apoptotic cells in a dose

dependent manner (**Fig. 7**). Control cells exposed to DMSO showed 1.97 % cells in sub G1 phase, whereas treated cells with compound **7c** showed a spike in the sub G1 population to 6.20% at 0.5 μ M, 30.93% at 1 μ M and 36.15% at 2.5 μ M concentration in 24 h. These results clearly demonstrate that **7c** induce apoptosis by sub G1 phase arrest of cell cycle.

<Insert Figure 7 here>

2.3.5. Mitochondrial Membrane Potential (MMP)

The hallmark of apoptosis is the loss of mitochondrial membrane potential. Mitochondria plays a major role in apoptosis corresponding to stress, and the loss of MMP is a signaling marker of early mitochondrial damage in the process of apoptosis. The study was performed using JC1 (a carbocyanine cationic dye) staining to detect the mitochondrial depolarization occurs during early stages of apoptosis in treated cells with compound **7c** at different concentrations of 0.5, 1 and 2.5 μ M. It shows potential based aggregation in mitochondria, as indicated by a fluorescence emission changes. Enhanced ROS levels induce the loss of MMP which further activates the apoptotic signalling and leads to cell death. The polarised cells mitochondria exhibits red colour (P1-phase) due to J-aggregates formation with it, whereas the depolarised cells mitochondria exhibits green colour (P2-phase) due to J-monomers formation [39]. The results from **Fig. 8** showed an increase in the apoptotic cell population of P2-phase (depolarized cell population) from 1.04% in control to 23.85% at 0.5 μ M, 52.80% at 1 μ M and 88.91% at 2.5 μ M. therefore, A-549 cells treated with compound **7c** for 24 hrs exhibited decreased MMP in dose dependent manner.

<Insert Figure 8 here>

2.3.6. AnnexinV/Propidium iodide dual staining assay

The percentage of apoptotic cells induced by compound **7c** can be easily calculated using Annexin V/Propidium iodide dual staining assay [40]. The Annexin V-Alexa Flour 488/PI dual staining assay provide detection of live cells (LL; AV-/PI-), early apoptotic cells (LR; AV+/PI-), late apoptotic cells (UR; AV+/PI+) and necrotic cells (UL; AV-/PI+). The results from **Fig. 9** showed that the compound **7c** induced the percentage of late apoptotic cells from 1.11% in control to 14.80% at 0.5 μ M, 31.41% at 1 μ M and 59.36% at 2.5 μ M respectively. Therefore, it is indicated that the compound **7c** induces apoptosis in A-549 cells in a dose dependent manner.

<Insert Figure 9 here>

2.3.7. Gal-1 ELISA enzymatic study with compound 7c

The Gal-1 levels in the healthy subjects are normal but it is upregulated in the tumour environment, and leads to cause tumour proliferation and metastasis. Therefore, Gal-1 is considered as a biomarker to target specific tumors like lung, breast, and prostate [41]. gal-1 quantitative enzyme immunoassay was performed to see the effectiveness of compound 7c on gal-1 levels in the process of apoptosis. The treated A-549 cells with compound 7c were incubated in 60mm cell culture dishes for 48 hrs, and the supernatant was collected. The expression of gal-1 can be quantified from the cellular external environment as gal-1 is an extracellular secreted protein. The collected equal quantities of supernatant were subjected to quantitative enzyme immunoassay as per manufacture's protocol [DGAL10, R&D Systems, USA]. The supernatant solutions were incubated with human gal-1coated plates, and washed to remove unbound protein. Furthermore, an enzyme attached antibody was added into the reaction, specific to human gal-1 and incubated with substrate solution about 30 minutes before terminating the reaction with 50 μ l of the stop solution. In the last stage, the quantification of protein expression was detected using UV-spectrophotometer. The results were stipulated in the graph (**Table 2**) and found to be a greater reduction in the gal-1 protein levels in dose dependent manner (**Fig. 10**) at the concentrations of 10, 30, 100 and 300 μ M. therefore, it is confirmed that the compound 7c significantly reduces the expression of gal-1.

<Insert Figure 10 here>

<Insert Table 2 here>

2.3.8. Fluorescence Spectroscopy (FS) study

The FS is a simple, sensitive and widely used technique to evaluate the interactions, and dynamics of proteins with ligands based on its fluorescence properties in solution. It provides binding affinity based on the protein–ligand interactions qualitatively and quantitatively in equilibrium conditions [42]. Fluorescence spectra of gal-1 in the increasing concentrations of ligand from 0 to 65 μ M at pH 7.5 was analysed, and the emission spectrum of gal-1 was achieved at 343 nm. It is noticed that there is a decrease in the fluorescence intensity of 7c with increasing its concentration (**Fig. 11A**). The graph of $\log[7c]$ versus $\log(F_0 - F)/F$ showed a linear relationship (**Fig. 11B**), and the total number of binding sites were found to be 1 based on the calculations from the slope, and concludes interaction of gal-1

protein and compound in 1:1 ratio. The binding constant (K_a) was calculated from the intercept value is $9.5 \times 10^3 \text{ M}^{-1}$. The intensity of the fluorescence was quenched upon increase of ligand concentration and the bimolar quenching constant (K_q) was calculated to be $1.4 \times 10^{12} \text{ M}^{-1} \text{ S}^{-1}$ which is larger than diffusion control limit suggesting interaction of gal-1 protein with ligand as well as the mode of quenching to be static.

<Insert Figure 11A & 11B here>

2.3.9. Surface Plasmon Resonance (SPR) studies

It is a spectroscopic technique which is used to detect protein interactions mainly binding of ligands in real-time without the use of labels by fixing or immobilizing the ligand on a thin metal film, and measuring the change in refractive index based on binding of the analyte. SPR instruments are primarily used to measure the binding kinetics and affinity of molecular interactions [43]. The gal-1 interaction with compound **7c** was analysed through SPR using immobilized gal-1 (ligand, 8070 RU) and compound **7c** (analyte) at various concentrations. Sensorgram was measured for each of concentration of compound **7c** (**Fig. 12**) and fitted using 1:1 interaction steady state affinity model. The equilibrium constant K_D value was found to be $1.19\text{E-}06 \text{ M}$ using Biacore T200 Evaluation software version 2.0. therefore, the SPR analysis showed interaction of gal-1 with compound **7c**, which is in validation with fluorescence studies.

<Insert Figure 12 here>

2.3.10. Molecular docking studies

To better understand the affinity of the compound **7c** with the active site of the gal-1, we have performed the molecular docking calculations using the Glide docking module of Schrodinger suite [44]. The 3D crystal co-ordinates of human gal-1 were obtained from the protein data bank (PDB ID: 4Y24). The 2D and 3D ligand interaction diagrams of compound **7c** are shown in **Fig. 13A, 13B & 13C**. Hydrogen bonding interaction was found at a distance of 1.75\AA between C=O of Glu71 acting as acceptor (atom no. 489) and the phenolic OH acting as donor (atom no. 2066). A π -cation interaction was found between NH of Lys63 (atom no. 464) and the phenyl ring of the N-benzyl substitution. Further, π - π stacking between the indole ring of Trp68 and phenyl ring connecting the benzimidazole with the triazole moiety and between imidazole moiety His44 and the benzimidazole moiety stabilize the docking pose of the **7c** molecule in the binding site.

A set of pharmacokinetic Absorption, Distribution, Metabolism, Elimination (ADMET) related properties of the molecule **7c** were calculated using qikprop [45]. The physicochemical properties of **7c** matched with the prescribed ranges as represented in **Table 3**. Additionally, the molecular weight (mol. Wt.), hydrogen bond donors (donor HB), hydrogen bond acceptors (accept HB), partition coefficient (QPlogPo/w), exhibited acceptable values that followed Lipinski rule of five.

<Insert Figure 13A, 13B & 13C here>

<Insert Table 3 here>

3. Conclusion

In conclusion, a series of benzimidazole-triazole hybrids have been synthesized and evaluated for their *in vitro* cytotoxic potential against various selected human cancer cell lines. The initial screening analysis showed that some of the derivatives were active against all selected cancer cell lines with IC₅₀ values below 10 μM. The *in vitro* screening results revealed the most active compound **7c** with broad range of activity against all the tested cell lines, and exhibited an excellent growth inhibition with an IC₅₀ of 0.63±0.21 μM against A-549 cell lines by inducing apoptosis *via* arresting cell cycle at Sub G1 phase, decreasing MMP, increasing apoptotic cells by Annexin V. The morphological changes like nuclear condensation, cell shrinkage, were observed through microscope DAPI staining, and also compound **7c** found to be non-toxic against normal NRK cells. The compound **7c** significantly reduced gal-1 protein expression in a dose dependent manner using enzymatic ELISA study. Further, the gal-1 interaction with compound **7c** was confirmed by surface plasmon resonance and fluorescence spectroscopy studies. Molecular docking studies also supported the possible mode of binding to the gal-1. we have succeeded in radiolabeling of **7c** with 18F radionuclide to prove as a PET tracer in addition to its potential cytotoxicity in low concentration. Overall, the current study indicates that these new series of benzimidazole-triazole hybrids have the potential to be advanced as gal-1 targeting cytotoxic agents as well as PET tracers for the diagnosis and, treatment of cancer.

4. Experimental protocols

4.1. Chemistry

All chemicals, reagents, and solvents were obtained from commercial suppliers, and used without further purification. Analytical thin layer chromatography (TLC) was performed on MERCK precoated silica gel 60-F₂₅₄ (0.5 mm) aluminum plates. Visualization

of the spots on TLC plates was achieved by UV light. $^1\text{H-NMR}$ & $^{13}\text{C-NMR}$ spectra were recorded on Bruker 500 MHz using DMSO or CDCl_3 solvent with tetramethyl silane (TMS) as the internal standard. Chemical shifts for ^1H & ^{13}C are reported in parts per million (ppm) towards higher values from TMS position. Spin-spin splitting pattern was mentioned as s (singlet), d (doublet), t (triplet), q (quartet), and m (multiplet). The coupling constant (J) values are mentioned in hertz (Hz). HRMS were calculated with Agilent QTOF mass spectrometer 6540 series instrument. Column chromatography was performed wherever required using silica gel 60-120 or 100-200 size. The evaporation of solvents was carried out under reduced pressure on Heidolph rotary evaporator below $50\text{ }^\circ\text{C}$.

4.1.1. Synthesis of N-benzyl-4-chloro-2-nitroaniline (3)

The 4-chloro-2-nitroaniline (1 eq) was added directly into water (10 mL) followed by added benzyl bromide (1.5 eq) and the reaction mixture was then stirred under reflux at $100\text{ }^\circ\text{C}$ for 3-4 hours. After confirmation by TLC the reaction mixture was removed and extracted with ethyl acetate (3x20 ml) and dried over Na_2SO_4 . The combined organic layer was concentrated in vacuo to give a red colour solid purified by column chromatography. Red solid, yield 85%; mp $186\text{-}188\text{ }^\circ\text{C}$; $^1\text{H NMR}$ (500 MHz, DMSO) δ 8.75 (t, $J = 6.0\text{ Hz}$, 1H), 8.07 (d, $J = 2.6\text{ Hz}$, 1H), 7.50 (dd, $J = 9.1, 2.4\text{ Hz}$, 1H), 7.37 – 7.33 (m, 4H), 7.28 – 7.24 (m, 1H), 6.94 (d, $J = 9.3\text{ Hz}$, 1H), 4.65 (d, $J = 6.2\text{ Hz}$, 2H). $^{13}\text{C NMR}$ (125 MHz, DMSO) δ 144.24, 138.64, 136.57, 131.68, 129.08, 127.59, 127.33, 125.44, 119.03, 117.49, 46.20.

4.1.2. Synthesis of N¹-benzyl-4-chlorobenzene-1,2-diamine (4)

Stannous chloride (5 eq) was added to a solution of N-benzyl-4-chloro-2-nitroaniline (3) in ethanol (5 ml) and the reaction mixture was stirred under reflux at $80\text{ }^\circ\text{C}$ for 5-6 hours. The reaction mixture was quenched with diluted NaHCO_3 and formed sticky emulsion type solution. It was filtered by suction filtration with celite bed on Buckner funnel to remove precipitate. Finally, the filtrate was extracted with ethyl acetate (3x20 ml) and dried over Na_2SO_4 . The combined organic layer was concentrated in vacuo to give a purple colour solid purified by column chromatography. Brown solid, yield 82%; mp $172\text{-}174\text{ }^\circ\text{C}$; $^1\text{H NMR}$ (500 MHz, DMSO) δ 7.41 – 7.10 (m, 5H), 6.57 (d, $J = 2.4\text{ Hz}$, 1H), 6.38 (dd, $J = 8.4, 2.4\text{ Hz}$, 1H), 6.27 (d, $J = 8.4\text{ Hz}$, 1H), 4.92 (s, 2H), 4.28 (d, $J = 5.8\text{ Hz}$, 2H). $^{13}\text{C NMR}$ (125 MHz, DMSO) δ 140.45, 137.51, 134.74, 128.73, 127.64, 127.12, 120.87, 116.56, 113.46, 111.41, 47.33.

4.1.3. Synthesis of 4-(1-benzyl-6-chloro-1H-benzo[d]imidazol-2-yl) phenol (5)

N1-benzyl-4-chlorobenzene-1, 2-diamine (4) (1 eq) was added to water and ethanol mixed solvent (1:1) and to this added sodium metabisulphite (15 eq) and finally added 4-hydroxy benzaldehyde (1 eq). The reaction mixture was stirred under reflux 80 °C for overnight. On cooling at room temperature 20-30 mL of cold water was added and stirred for 10 min. The solid separated out was filtered at pump and dried. The residues were purified by column chromatography on silica gel. White solid, yield 85%; mp 242-244 °C; ¹H NMR (500 MHz, DMSO) δ 10.03 (s, 1H), 7.74 (d, *J* = 1.9 Hz, 1H), 7.59 – 7.55 (m, 2H), 7.45 (d, *J* = 8.6 Hz, 1H), 7.30 (t, *J* = 7.3 Hz, 2H), 7.27 – 7.21 (m, 2H), 6.99 (d, *J* = 7.2 Hz, 2H), 6.89 (d, *J* = 8.2 Hz, 2H), 5.57 (s, 2H). ¹³C NMR (125 MHz, DMSO) δ 159.61, 155.66, 144.08, 137.18, 135.25, 131.08, 129.28, 127.99, 126.97, 126.55, 122.77, 120.67, 118.80, 116.10, 112.73, 48.12.

4.1.4. Synthesis of 1-benzyl-6-chloro-2-(4-(prop-2-yn-1-yloxy) phenyl)-1H benzo[d]imidazole (6)

To the solution of compound 5 (1 mmol) in freshly distilled acetone (10 mL), added anhydrous K₂CO₃ (2.5 mmol) as a base and propargyl bromide (1 mmol) was added drop wise and stirred under reflux for 2-3 hr. The solvent was evaporated completely and the obtained residue was extracted with ethyl acetate (3x20 mL) and dried over Na₂SO₄. The combined organic layer was concentrated in vacuo and the residues were purified by column chromatography on silica gel. White solid, yield 81%; mp 256-258 °C; ¹H NMR (500 MHz, DMSO) δ 7.77 (d, *J* = 2.0 Hz, 1H), 7.72 – 7.69 (m, 2H), 7.48 (d, *J* = 8.6 Hz, 1H), 7.32 – 7.28 (m, 2H), 7.27 – 7.23 (m, 2H), 7.15 – 7.12 (*J* = 8.0 Hz, 2H), 7.00 (d, *J* = 7.2 Hz, 2H), 5.60 (s, 2H), 4.89 (d, *J* = 2.4 Hz, 2H), 3.62 (t, *J* = 2.3 Hz, 1H). ¹³C NMR (125 MHz, DMSO) δ 159.04, 155.07, 144.05, 137.10, 135.28, 130.97, 129.32, 128.02, 127.12, 126.51, 123.03, 118.99, 115.64, 112.83, 79.37, 79.00, 56.11, 48.15.

4.1.5. General procedure for the synthesis of final compounds 7a-t.

A 50 mL round bottom flask was charged with 1-benzyl-6-chloro-2-(4-(prop-2-yn-1-yloxy) phenyl)-1H-benzo[d]imidazole (1 mmol), various phenyl and, benzyl azides (0.9 mmol), sodium ascorbate (0.3 mmol), 2 mL of ethanol and 2 mL of distilled water. Then, CuSO₄·5H₂O (0.15 mmol) was added. The reaction mixture was stirred under rt for overnight. After completion of the reaction by TLC analysis, the mixture was filtered and extracted with ethyl acetate (3x20 ml) and dried over Na₂SO₄. The combined organic layer

was concentrated in vacuo and the residues were purified by column chromatography on silica gel, offered the final target compounds 7a-t with moderate to good yields.

4.1.5.1. 1-benzyl-5-chloro-2-(4-((1-phenyl-1H-1,2,3-triazol-4-yl) methoxy) phenyl)-1H-benzo[d]imidazole (7a)

White solid, yield 83%; mp 287-289 °C; ¹H NMR (500 MHz, DMSO) δ 8.97 (s, 1H), 7.91 (d, *J* = 6.1 Hz, 2H), 7.78 – 7.71 (m, 3H), 7.62 (s, 2H), 7.51 (d, *J* = 6.9 Hz, 2H), 7.29 (d, *J* = 6.1 Hz, 2H), 7.22 – 7.16 (m, 4H), 7.00 (s, 2H), 5.60 (s, 2H), 5.33 (s, 2H). ¹³C NMR (125 MHz, DMSO) δ 159.86, 144.03, 136.97, 131.02, 130.93, 130.40, 129.31, 128.07, 127.14, 126.52, 123.50, 123.12, 122.74, 120.70, 119.19, 119.00, 118.96, 115.66, 115.62, 112.95, 61.63, 48.23. HRMS (ESI): *m/z* calcd for C₂₉H₂₂ClN₅O, 491. 1513, found 492.1597 [M+H]⁺.

4.1.5.2. 1-benzyl-5-chloro-2-(4-((1-(2-methoxyphenyl)-1H-1,2,3-triazol-4-yl) methoxy) phenyl)-1H-benzo[d]imidazole (7b)

White solid, yield 85%; mp 310-312 °C; ¹H NMR (500 MHz, DMSO) δ 8.61 (s, 1H), 7.74 (d, *J* = 15.2 Hz, 3H), 7.63 (d, *J* = 7.2 Hz, 1H), 7.54 (d, *J* = 6.4 Hz, 2H), 7.35 – 7.19 (m, 7H), 7.15 (t, *J* = 7.3 Hz, 1H), 7.00 (d, *J* = 6.4 Hz, 2H), 5.60 (s, 2H), 5.30 (s, 2H), 3.85 (s, 3H). ¹³C NMR (125 MHz, DMSO) δ 160.04, 152.14, 142.65, 136.97, 136.90, 131.32, 131.06, 129.32, 128.09, 127.29, 127.28, 127.25, 126.56, 126.25, 126.09, 123.31, 121.39, 118.99, 118.91, 115.61, 113.54, 113.08, 61.58, 56.61, 48.29. HRMS (ESI): *m/z* calcd for C₃₀H₂₄ClN₅O₂, 521. 1619, found 522.1700 [M+H]⁺.

4.1.5.3. 3-(4-((4-(1-benzyl-5-chloro-1H-benzo[d]imidazol-2-yl) phenoxy) methyl)-1H-1,2,3-triazol-1-yl) phenol (7c)

Light yellow solid, yield 81%; mp 274-276 °C; ¹H NMR (500 MHz, DMSO) δ 10.06 (s, 1H), 8.92 (s, 1H), 7.75 – 7.70 (m, 3H), 7.54 (s, 1H), 7.35 – 7.30 (m, 6H), 7.26 – 7.24 (m, 3H), 6.95 (d, *J* = 48.0 Hz, 3H), 5.60 (s, 2H), 5.30 (s, 2H). ¹³C NMR (125 MHz, DMSO) δ 159.93, 158.97, 143.87, 138.01, 136.94, 131.24, 130.99, 129.30, 128.06, 127.19, 126.56, 123.46, 123.25, 122.63, 119.01, 116.25, 115.58, 113.08, 111.04, 107.64, 61.66, 48.34. HRMS (ESI): *m/z* calcd for C₂₉H₂₂ClN₅O₂, 507. 1462, found 508.1551 [M+H]⁺.

4.1.5.4. 1-benzyl-5-chloro-2-(4-((1-(p-tolyl)-1H-1,2,3-triazol-4-yl) methoxy) phenyl)-1H-benzo[d]imidazole (7d)

White solid, yield 82%; mp 293-295 °C; ¹H NMR (500 MHz, DMSO) δ 8.92 (s, 1H), 7.75 (d, *J* = 34.9 Hz, 5H), 7.55 – 7.15 (m, 9H), 7.00 (s, 2H), 5.60 (s, 2H), 5.31 (s, 2H), 2.38 (s, 3H). ¹³C NMR (125 MHz, DMSO) δ 159.87, 144.09, 143.91, 138.91, 137.09, 134.81, 131.04, 130.71, 129.31, 128.03, 127.09, 126.54, 123.37, 123.04, 122.80, 120.56, 119.01, 115.59, 112.89, 61.71, 48.20, 21.03. HRMS (ESI): *m/z* calcd for C₃₀H₂₄ClN₅O, 505. 1669, found 506.1755 [M+H]⁺.

4.1.5.5. 1-benzyl-5-chloro-2-(4-((1-(4-(trifluoromethyl) phenyl)-1H-1,2,3-triazol-4-yl) methoxy) phenyl)-1H-benzo[d]imidazole (7e)

Brown solid, yield 79%; mp 273-275 °C; ¹H NMR (500 MHz, DMSO) δ 9.14 (s, 1H), 8.19 (d, *J* = 8.4 Hz, 2H), 8.01 (d, *J* = 8.5 Hz, 2H), 7.76 (d, *J* = 27.5 Hz, 3H), 7.51 (d, *J* = 8.0 Hz, 1H), 7.30 (t, *J* = 7.3 Hz, 2H), 7.25 (d, *J* = 7.5 Hz, 4H), 7.00 (d, *J* = 7.3 Hz, 2H), 5.61 (s, 2H), 5.35 (s, 2H). ¹³C NMR (125 MHz, DMSO) δ 159.82, 144.46, 139.82, 137.06, 131.01, 129.43, 129.31, 129.17, 128.02, 127.70, 127.67, 127.06, 126.54, 125.36, 123.77, 123.20, 123.07, 121.15, 119.09, 115.61, 112.98, 61.64, 48.29. HRMS (ESI): *m/z* calcd for C₃₀H₂₁ClF₃N₅O, 559. 1387, found 560.1481 [M+H]⁺.

4.1.5.6. 1-benzyl-5-chloro-2-(4-((1-(4-fluorophenyl)-1H-1,2,3-triazol-4-yl) methoxy) phenyl)-1H-benzo[d]imidazole (7f)

Light brown solid, yield 80%; mp 251-253 °C; ¹H NMR (500 MHz, DMSO) δ 8.96 (s, 1H), 7.96 (d, *J* = 8.4 Hz, 2H), 7.75 (d, *J* = 24.1 Hz, 3H), 7.52 (d, *J* = 7.7 Hz, 1H), 7.47 (t, *J* = 8.6 Hz, 2H), 7.30 – 7.26 (m, 3H), 7.25 (d, *J* = 9.6 Hz, 3H), 7.00 (d, *J* = 7.2 Hz, 2H), 5.60 (s, 2H), 5.32 (s, 2H). ¹³C NMR (126 MHz, DMSO) δ 163.18, 161.23, 159.94, 144.04, 136.95, 133.61, 131.06, 129.31, 128.06, 127.26, 126.56, 123.75, 123.26, 123.11, 123.04, 122.59, 118.92, 117.30, 117.11, 115.59, 113.04, 61.69, 48.29. HRMS (ESI): *m/z* calcd for C₂₉H₂₁ClFN₅O, 509. 1419, found 510.1496 [M+H]⁺.

4.1.5.7. 1-benzyl-5-chloro-2-(4-((1-(3-fluorophenyl)-1H-1,2,3-triazol-4-yl) methoxy) phenyl)-1H-benzo[d]imidazole (7g)

Light brown solid, yield 81%; mp 247-249 °C; ¹H NMR (500 MHz, DMSO) δ 9.04 (s, 1H), 7.87 (d, *J* = 10.1 Hz, 1H), 7.82 (d, *J* = 8.1 Hz, 2H), 7.71 (d, *J* = 20.3 Hz, 2H), 7.70 – 7.63 (m, 1H), 7.53 (s, 1H), 7.38 (t, *J* = 7.2 Hz, 1H), 7.33 – 7.20 (m, 6H), 6.99 (d, *J* = 6.9 Hz, 2H), 5.61 (s, 2H), 5.33 (s, 2H). ¹³C NMR (125 MHz, DMSO) δ 163.86, 161.91, 159.87, 144.23, 138.26, 136.93, 132.39, 132.32, 130.99, 129.31, 128.07, 127.15, 126.55, 123.69, 123.23,

119.07, 116.62, 116.10, 115.93, 115.62, 113.11, 108.29, 108.08, 61.63, 48.38. HRMS (ESI): m/z calcd for $C_{29}H_{21}ClFN_5O$, 509. 1419, found 510.1504 $[M+H]^+$.

4.1.5.8. 1-benzyl-2-(4-((1-(4-bromophenyl)-1H-1,2,3-triazol-4-yl) methoxy) phenyl)-5-chloro-1H-benzo[d]imidazole (7h)

Light red solid, yield 84%; mp 269-271 °C; 1H NMR (500 MHz, DMSO) δ 9.01 (s, 1H), 7.90 (d, $J = 8.4$ Hz, 2H), 7.82 (d, $J = 8.4$ Hz, 2H), 7.75 (d, $J = 27.7$ Hz, 3H), 7.49 (d, $J = 8.1$ Hz, 1H), 7.29 (d, $J = 7.2$ Hz, 2H), 7.24 (t, $J = 8.2$ Hz, 4H), 7.00 (d, $J = 7.0$ Hz, 2H), 5.60 (s, 2H), 5.32 (s, 2H). ^{13}C NMR (125 MHz, DMSO) δ 159.83, 144.22, 137.08, 136.24, 133.27, 131.05, 129.31, 128.03, 127.10, 126.53, 123.53, 123.04, 122.83, 122.60, 121.93, 119.01, 115.59, 112.89, 61.66, 48.20. HRMS (ESI): m/z calcd for $C_{29}H_{21}BrClN_5O$, 569. 8750, found 572.0687 $[M+2]^+$.

4.1.5.9. 1-benzyl-5-chloro-2-(4-((1-(2-chloro-4-nitrophenyl)-1H-1,2,3-triazol-4-yl) methoxy) phenyl)-1H-benzo[d]imidazole (7i)

White solid, yield 81%; mp 315-217 °C; 1H NMR (500 MHz, DMSO) δ 8.88 (s, 1H), 8.64 (d, $J = 2.0$ Hz, 1H), 8.41 (dd, $J = 8.7, 2.0$ Hz, 1H), 8.06 (d, $J = 8.7$ Hz, 1H), 7.82 – 7.66 (m, 3H), 7.50 (d, $J = 8.3$ Hz, 1H), 7.34 – 7.21 (m, 6H), 7.00 (d, $J = 7.3$ Hz, 2H), 5.61 (s, 2H), 5.37 (s, 2H). ^{13}C NMR (125 MHz, DMSO) δ 159.84, 148.80, 143.43, 139.56, 137.05, 131.03, 129.77, 129.73, 129.32, 128.05, 127.45, 127.12, 126.54, 126.35, 124.05, 123.09, 122.85, 119.02, 115.62, 112.95, 61.43, 48.23. HRMS (ESI): m/z calcd for $C_{29}H_{20}Cl_2N_6O_3$, 570. 0974, found 571.1061 $[M+H]^+$.

4.1.5.10. 1-benzyl-5-chloro-2-(4-((1-(4-methyl-3-nitrophenyl)-1H-1,2,3-triazol-4-yl) methoxy) phenyl)-1H-benzo[d]imidazole (7j)

Off White solid, yield 82%; mp 295-297 °C; 1H NMR (500 MHz, DMSO) δ 9.12 (s, 1H), 8.54 (s, 1H), 8.21 (d, $J = 7.2$ Hz, 1H), 7.84 – 7.64 (m, 4H), 7.53 (d, $J = 7.4$ Hz, 1H), 7.33 – 7.15 (m, 6H), 7.00 (d, $J = 6.9$ Hz, 2H), 5.60 (s, 2H), 5.34 (s, 2H), 2.59 (s, 3H). ^{13}C NMR (125 MHz, DMSO) δ 159.93, 149.74, 144.33, 136.88, 135.49, 134.80, 134.58, 133.46, 131.05, 129.31, 128.08, 127.32, 126.57, 124.78, 123.76, 123.37, 122.54, 118.92, 116.28, 115.57, 113.15, 61.63, 48.35, 19.57. HRMS (ESI): m/z calcd for $C_{30}H_{23}ClN_6O_3$, 550. 1520, found 551.1604 $[M+H]^+$.

4.1.5.11. 1-benzyl-5-chloro-2-(4-((1-(3-nitrophenyl)-1H-1,2,3-triazol-4-yl) methoxy) phenyl)-1H-benzo[d]imidazole (7k)

White solid, yield 85%; mp 285-287 °C; ¹H NMR (500 MHz, DMSO) δ 9.22 (s, 1H), 8.75 (t, *J* = 2.1 Hz, 1H), 8.43 (dd, *J* = 8.1, 1.4 Hz, 1H), 8.35 (dd, *J* = 8.2, 1.6 Hz, 1H), 7.92 (t, *J* = 8.2 Hz, 1H), 7.79 – 7.69 (m, 3H), 7.49 (d, *J* = 8.5 Hz, 1H), 7.31 – 7.24 (m, 6H), 7.01 (d, *J* = 7.3 Hz, 2H), 5.59 (s, 2H), 5.36 (s, 2H). ¹³C NMR (125 MHz, DMSO) δ 159.81, 159.06, 149.02, 144.48, 137.60, 137.06, 132.02, 131.06, 130.95, 129.32, 128.03, 127.12, 126.68, 126.53, 123.98, 123.69, 123.09, 122.80, 118.98, 115.63, 115.60, 115.39, 112.92, 61.62, 48.20. HRMS (ESI): *m/z* calcd for C₂₉H₂₁ClN₆O₃, 536. 1364, found 537.1443 [M+H]⁺.

4.1.5.12. 1-benzyl-2-(4-((1-benzyl-1H-1,2,3-triazol-4-yl) methoxy) phenyl)-5-chloro-1H-benzo[d]imidazole (7l)

Off white solid, yield 86%; mp 252-254 °C; ¹H NMR (500 MHz, DMSO) δ 8.31 (s, 1H), 7.77 (s, 1H), 7.68 (d, *J* = 7.8 Hz, 2H), 7.48 (d, *J* = 8.2 Hz, 1H), 7.37 (d, *J* = 6.8 Hz, 2H), 7.36 – 7.27 (m, 5H), 7.26 (d, *J* = 5.9 Hz, 2H), 7.18 (d, *J* = 7.8 Hz, 2H), 7.00 (d, *J* = 7.1 Hz, 2H), 5.62 (s, 2H), 5.59 (s, 2H), 5.22 (s, 2H). ¹³C NMR (125 MHz, DMSO) δ 159.90, 159.05, 144.04, 143.16, 137.08, 136.44, 131.00, 129.32, 129.24, 128.64, 128.44, 128.04, 127.10, 126.52, 125.31, 123.05, 122.62, 118.98, 115.64, 115.53, 112.90, 61.72, 53.36, 48.17. HRMS (ESI): *m/z* calcd for C₃₀H₂₄ClN₅O, 505. 1669, found 506.1752 [M+H]⁺.

4.1.5.13. 1-benzyl-5-chloro-2-(4-((1-(2-nitrobenzyl)-1H-1,2,3-triazol-4-yl) methoxy) phenyl)-1H-benzo[d]imidazole (7m)

White solid, yield 85%; mp 291-293 °C; ¹H NMR (500 MHz, DMSO) δ 8.31 (s, 1H), 8.15 (d, *J* = 8.0 Hz, 1H), 7.81 – 7.68 (m, 4H), 7.64 (t, *J* = 7.6 Hz, 1H), 7.50 (d, *J* = 7.4 Hz, 1H), 7.30 (t, *J* = 7.1 Hz, 2H), 7.26 (d, *J* = 6.6 Hz, 2H), 7.20 (d, *J* = 7.0 Hz, 2H), 7.09 (d, *J* = 7.5 Hz, 1H), 7.00 (d, *J* = 7.1 Hz, 2H), 5.99 (s, 2H), 5.59 (s, 2H), 5.26 (s, 2H). ¹³C NMR (125 MHz, DMSO) δ 159.88, 159.07, 148.08, 143.18, 137.02, 134.82, 131.17, 130.98, 130.65, 130.17, 129.32, 128.05, 127.13, 126.53, 126.11, 125.55, 123.11, 122.61, 119.00, 115.64, 115.59, 112.98, 61.68, 56.09, 50.48. HRMS (ESI): *m/z* calcd for C₃₀H₂₃ClN₆O₃, 550. 1520, found 551.1600 [M+H]⁺.

4.1.5.14. 1-benzyl-5-chloro-2-(4-((1-(4-nitrobenzyl)-1H-1,2,3-triazol-4-yl) methoxy) phenyl)-1H-benzo[d]imidazole (7n)

Off White solid, yield 84%; mp 287-289 °C; ¹H NMR (500 MHz, DMSO) δ 8.39 (s, 1H), 8.24 (d, *J* = 8.4 Hz, 2H), 7.70 – 7.62 (m, 3H), 7.55 (d, *J* = 8.5 Hz, 3H), 7.30 – 7.24 (m, 4H), 7.18 (s, 2H), 6.99 (d, *J* = 7.3 Hz, 2H), 5.82 (s, 2H), 5.59 (s, 2H), 5.23 (s, 2H). ¹³C NMR (125 MHz, DMSO) δ 160.08, 147.76, 143.78, 136.72, 130.97, 129.54, 129.31, 128.13, 127.42, 126.59, 125.85, 124.39, 123.59, 122.27, 118.97, 118.90, 115.56, 113.37, 67.40, 61.73, 52.48. HRMS (ESI): *m/z* calcd for C₃₀H₂₃ClN₆O₃, 550. 1520, found 551.1591 [M+H]⁺.

4.1.5.15. 1-benzyl-5-chloro-2-(4-((1-(2-fluorobenzyl)-1H-1,2,3-triazol-4-yl) methoxy) phenyl)-1H-benzo[d]imidazole (7o)

Light brown solid, yield 82%; mp 268-270 °C; ¹H NMR (500 MHz, DMSO) δ 8.32 (d, *J* = 26.8 Hz, 1H), 7.77 (s, 1H), 7.69 (d, *J* = 8.0 Hz, 2H), 7.48 (d, *J* = 8.6 Hz, 1H), 7.45 – 7.38 (m, 1H), 7.30 (t, *J* = 7.2 Hz, 2H), 7.24 (dd, *J* = 15.9, 7.7 Hz, 3H), 7.20 – 7.13 (m, 4H), 7.00 (d, *J* = 7.2 Hz, 2H), 5.67 (d, *J* = 16.5 Hz, 2H), 5.59 (s, 2H), 5.23 (d, *J* = 4.6 Hz, 2H). ¹³C NMR (125 MHz, DMSO) δ 159.88, 144.05, 143.24, 143.07, 139.12, 139.06, 137.10, 131.37, 131.01, 129.32, 128.03, 127.09, 126.52, 125.45, 124.52, 123.01, 122.66, 118.97, 115.53, 115.24, 112.87, 61.71, 61.66, 52.67, 48.15. HRMS (ESI): *m/z* calcd for C₃₀H₂₂ClFN₅O, 523. 1575, found 524.1660 [M+H]⁺.

4.1.5.16. 1-benzyl-5-chloro-2-(4-((1-(3,5-difluorobenzyl)-1H-1,2,3-triazol-4-yl) methoxy) phenyl)-1H-benzo[d]imidazole (7p)

Brown solid, yield 80%; mp 264-266 °C; ¹H NMR (500 MHz, DMSO) δ 8.37 (s, 1H), 7.77 (s, 1H), 7.69 (d, *J* = 7.6 Hz, 2H), 7.48 (d, *J* = 8.5 Hz, 1H), 7.30 (t, *J* = 7.2 Hz, 2H), 7.28 – 7.22 (m, 3H), 7.19 (d, *J* = 8.1 Hz, 2H), 7.06 (d, *J* = 6.3 Hz, 2H), 7.00 (d, *J* = 7.2 Hz, 2H), 5.67 (s, 2H), 5.59 (s, 2H), 5.24 (s, 2H). ¹³C NMR (125 MHz, DMSO) δ 159.87, 144.07, 143.32, 140.60, 137.10, 131.01, 129.31, 128.03, 127.08, 126.53, 125.57, 123.01, 122.71, 118.97, 115.55, 112.86, 111.89, 111.84, 111.73, 111.68, 104.42, 104.21, 104.01, 61.72, 52.25, 48.15. HRMS (ESI): *m/z* calcd for C₃₀H₂₂ClF₂N₅O, 541. 1481, found 542.1558 [M+H]⁺.

4.1.5.17. 1-benzyl-2-(4-((1-(4-bromobenzyl)-1H-1,2,3-triazol-4-yl) methoxy) phenyl)-5-chloro-1H-benzo[d]imidazole (7q)

Light red solid, yield 81%; mp 281-283 °C; ¹H NMR (500 MHz, DMSO) δ 8.32 (s, 1H), 7.77 (s, 1H), 7.69 (d, *J* = 7.5 Hz, 2H), 7.59 (d, *J* = 7.9 Hz, 2H), 7.48 (d, *J* = 8.4 Hz, 1H), 7.32 – 7.23 (m, 6H), 7.18 (d, *J* = 7.8 Hz, 2H), 7.00 (d, *J* = 7.0 Hz, 2H), 5.61 (s, 2H), 5.59 (s,

2H), 5.22 (s, 2H). ^{13}C NMR (125 MHz, DMSO) δ 159.87, 144.08, 143.22, 137.10, 135.84, 132.18, 131.00, 130.69, 129.32, 128.03, 127.08, 126.52, 125.37, 123.01, 122.68, 121.94, 118.98, 115.55, 112.87, 61.71, 52.60, 48.16. HRMS (ESI): m/z calcd for $\text{C}_{30}\text{H}_{23}\text{BrClN}_5\text{O}$, 584. 9020, found 586.0839 $[\text{M}+2]^+$.

4.1.5.18. 1-benzyl-2-(4-((1-(2-bromobenzyl)-1H-1,2,3-triazol-4-yl) methoxy) phenyl)-5-chloro-1H-benzo[d]imidazole (7r)

Light red solid, yield 83%; mp 290-292 $^{\circ}\text{C}$; ^1H NMR (500 MHz, DMSO) δ 8.35 (s, 1H), 7.75 (s, 1H), 7.69 (d, $J = 7.9$ Hz, 2H), 7.55 (d, $J = 11.3$ Hz, 2H), 7.48 (d, $J = 8.5$ Hz, 1H), 7.39 – 7.30 (m, 4H), 7.27 – 7.22 (m, 2H), 7.19 (d, $J = 8.1$ Hz, 2H), 7.00 (d, $J = 7.3$ Hz, 2H), 5.64 (s, 2H), 5.59 (s, 2H), 5.23 (s, 2H). ^{13}C NMR (125 MHz, DMSO) δ 159.89, 144.01, 143.25, 139.05, 137.08, 131.54, 131.45, 131.23, 131.00, 129.32, 128.04, 127.57, 127.11, 126.53, 125.47, 123.04, 122.63, 122.33, 118.97, 115.64, 115.53, 112.89, 61.71, 52.51, 48.18. HRMS (ESI): m/z calcd for $\text{C}_{30}\text{H}_{23}\text{BrClN}_5\text{O}$, 584. 9020, found 586.0840 $[\text{M}+2]^+$.

4.1.5.19. 1-benzyl-5-chloro-2-(4-((1-(2,3-dimethylphenyl)-1H-1,2,3-triazol-4-yl) methoxy) phenyl)-1H-benzo[d]imidazole (7s)

White solid, yield 85%; mp 298-300 $^{\circ}\text{C}$; ^1H NMR (500 MHz, DMSO) δ 8.57 (s, 1H), 7.77 (s, 1H), 7.71 (d, $J = 7.6$ Hz, 2H), 7.49 (d, $J = 8.5$ Hz, 1H), 7.41 (d, $J = 7.2$ Hz, 1H), 7.30 (d, $J = 7.2$ Hz, 3H), 7.30 – 7.21 (m, 5H), 7.01 (d, $J = 7.0$ Hz, 2H), 5.60 (s, 2H), 5.33 (s, 2H), 2.35 (s, 3H), 1.94 (s, 3H). ^{13}C NMR (125 MHz, DMSO) δ 159.89, 144.04, 142.91, 138.95, 137.09, 136.77, 132.68, 131.67, 131.04, 129.32, 128.04, 127.18, 127.10, 126.69, 126.54, 124.46, 123.04, 122.73, 118.97, 115.64, 112.89, 61.66, 48.16, 20.34, 14.33. HRMS (ESI): m/z calcd for $\text{C}_{31}\text{H}_{26}\text{ClN}_5\text{O}$, 519. 1826, found 520.1911 $[\text{M}+\text{H}]^+$.

4.1.5.20. 1-benzyl-5-chloro-2-(4-((1-(naphthalen-1-yl)-1H-1,2,3-triazol-4-yl) methoxy) phenyl)-1H-benzo[d]imidazole (7t)

Off white solid, yield 80%; mp 311-313 $^{\circ}\text{C}$; ^1H NMR (500 MHz, DMSO) δ 8.82 (s, 1H), 8.18 (dd, $J = 36.0, 8.1$ Hz, 2H), 7.82 – 7.59 (m, 7H), 7.49 (dd, $J = 16.4, 8.4$ Hz, 2H), 7.34 – 7.20 (m, 6H), 7.01 (d, $J = 7.2$ Hz, 2H), 5.61 (s, 2H), 5.40 (s, 2H). ^{13}C NMR (125 MHz, DMSO) δ 159.98, 159.09, 143.80, 143.14, 137.03, 134.14, 133.64, 131.08, 130.97, 130.84, 129.32, 128.85, 128.51, 128.41, 128.06, 127.98, 127.62, 127.20, 126.55, 125.91, 124.47, 123.16, 122.61, 122.33, 118.93, 115.64, 112.96, 61.70, 48.21. HRMS (ESI): m/z calcd for $\text{C}_{33}\text{H}_{24}\text{ClN}_5\text{O}$, 541. 1669, found 542.1776 $[\text{M}+\text{H}]^+$.

4.2. Radiochemistry

4.2.1 General Procedure:

All the chemicals, and solvents were procured from Loba chemie, India. The analytical techniques were used for quality control studies like Gas chromatography (Scion 436 GC, Netherlands) with flame ionization detector (FID), High performance liquid chromatography (HPLC) system (Dionex, ICS- 5000+, +, California. USA), Dose calibrator (Capintec CRC-25PET, New Jersey. USA), Radio Thin layer chromatography (Radio TLC) scanner (EZ-SCAN, California, USA) with multimode radiation detector (OMNI-RAD, California. USA), pH paper (Fisher Scientific, New Hampshire. USA). The ^{18}F radionuclide was produced with 16.5MeV in-house Cyclotron (PETtrace 860, GE Healthcare, USA) by the proton bombardment on the enriched ^{18}O water using $^{18}\text{O}(\text{p}, \text{n})^{18}\text{F}$ reaction. The proton bombardment was carried out with the beam current of range of 30 μA -65 μA for 10-15 min, which depend on the requirement of ^{18}F radioisotope. The radiolabeling was performed with the produced ^{18}F in the semiautomatic synthesizer module i.e., Tracerlab FX2N, GE Healthcare, Chicago. USA using the Helium (UHP-5.5) as a carrier gas.

4.2.2 Radio synthesis of target compound

A stock solution for ^{18}F radioisotope eluent was made by adding 12 mg of potassium carbonate and 60 mg of Kryptofix (K222) into a small beaker containing 12 ml of acetonitrile and 525 μL of the deionized water. The ^{18}F was eluted from conditioned QMA (4 ml ethanol followed by 10 ml water) cartridge through a mixture of QMA eluent stock solution (1.5 mL), and acetonitrile (0.5 mL) into the reactor vessel. Initially, the $[\text{K} 2.2.2] \text{K}^+ [^{18}\text{F}]^-$ complex was dried and, the reaction with the precursor (5 ± 0.5 mg,) in 1.5 ml of DMF was carried out at 160°C for 30 min. After completion of the reaction, the reaction mixture was diluted with acidic water (5 mL, $\text{pH}=3.0$) and passed through tC18 light cartridge for primary purification. The cartridge was washed with 5 mL of water, and 4 mL of 8% ethanol. The final purification was performed using 3 mL of 20-100% ethanol.

4.2.3. Quality control parameters

The radiochemical purity, identity & residual solvent limits of the final ^{18}F -7c preparation was determined by High-Performance Liquid Chromatography (HPLC), Thin-Layer Chromatography (TLC), and Gas Chromatography (GC). In TLC study, 5 μL of sample was spotted on TLC plate above the mobile phase level and run the TLC using acetonitrile/saline

(1:1). In HPLC study, gradient method was used for better resolution of peaks on the spectra. The gradient method was started with 5% acetonitrile (0-2.5 min), 5% to 100% acetonitrile (2.5-10 min), then 100% acetonitrile (10-12.5 min) and again at 5% acetonitrile (21.5-15min) with a flow rate of 2 mL/min. The C18 column (250 mm X 4.6 mm, 5 μ m) was used, and UV detection wavelength (λ_{max}) was 280 nm. In GC study, 1 μ L sample was injected into the injector, the column (BR-200ms, 0.32 mm ID) was operated at 40°C for initial 3 min followed by 50°C/min up to 8 min, and the temperature was set at 240°C and, the makeup gas consists of Helium (28 mL/min), hydrogen gas (30 mL/min), and zero air (300 mL/min) at the flow rate of 2 mL/min.

4.3. Biology

4.3.1. Cell Culture

Cells were procured from National Centre for Cell Science (NCCS) Pune, India and stocks were maintained in the sterile laboratory conditions. breast (MCF-7 and MDA-MB-231) lung (A-549 and NCI-H460), and Human keratinocyte (HaCaT) cancer cells were grown in tissue culture flasks in DMEM (Dulbecco modified Eagle medium, Sigma) or MEM (Minimum Essential Medium, Sigma) supplemented with 10% fetal bovine serum with 1X stabilized antibiotic-antimycotic solution (Sigma) in a CO₂ incubator at 37 °C with 5% CO₂ and 90% relative humidity.

4.3.2. MTT assay

For all the synthesized compounds **7a-t**. The anticancer activity was determined using MTT assay. 1×10^4 cells per well were seeded, supplemented with 10% FBS in each well of 96-well microculture plates and incubated for 48 h, at 37 °C in a CO₂ incubator. Compounds, diluted to the required concentrations in culture medium, were added to the wells with respective vehicle control. After 48 h of incubation, 10 μ L MTT (3-(4,5-dimethylthiazol-2-yl)-2,5-diphenyl tetrazolium bromide) (5 mg/mL) was added to all the plates and incubated for 4 h. Then, the supernatant from each well was carefully decanted, formazon crystals were dissolved in 100 μ L of DMSO and absorbance was recorded at 570 nm wavelength.

4.3.3. DAPI staining

A-549 cells were cultured in 12-well plates and treated with 0.5, 1 and 2.5 μ M of compound **7c**. The untreated and treated cells were washed two times with PBS, followed by fixation with 4% paraformaldehyde and staining with 10 μ g/mL of DAPI. The cells were observed

for apoptotic characteristics under fluorescence microscope (Nikon, Inc. Japan) with excitation at 359 nm and emission at 461 nm using DAPI filter at 200X magnification.

4.3.4. Cell cycle analysis

A-549 cells (1×10^6 cells/well) in 6 well plate were treated with different 0.25, 1 and 2.5 μM concentrations of the compound **7c** for 24 h and cells were collected by trypsinisation, washed with 150 mM PBS and were fixed with 70% ethanol for 30 min at 4 °C. after fixing, cells were washed with PBS and stained with 400 μL of propidium iodide staining buffer [PI (200 μg), Triton X (100 μL), DNase-free RNase A (2 mg) in 10 mL PBS] for 15 min at room temp in dark. The samples were then analyzed for propidium iodide fluorescence from 15,000 events by flow cytometry using BD Accuri C6 flow-cytometer.

4.3.5. Measurement of mitochondrial membrane potential ($D\Psi\text{m}$)

A-549 cells were cultured in 6 well plates at 5×10^5 cells/mL density and allowed to adhere overnight. The cells were treated with 0.5, 1 and 2.5 μM concentrations of compound **7c** for 24h. After 24h of compound treatment, the adherent cells were collected by trypsinisation, washed with PBS and resuspended in solution of PBS containing rhodamine-123 (10 $\mu\text{g}/\text{mL}$) and further incubated at room temperature for 30 minutes. Cells were washed with PBS to remove excess dye and resuspended in PBS. The samples were analyzed for rhodamine-123 fluorescence using spectrofluorometer with an excitation and emission wavelengths of 480 and 530 nm.

4.3.6. Annexin V-FITC/Propidium iodide dual staining assay

The Annexin V-FITC/Propidium iodide dual staining assay was performed using A-549 cells. To quantify the percentage of apoptotic cells, A-549 cells (1×10^6 mL per well) were plated in six-well culture plates and allowed to grow for 24 h. after treatment with increasing concentrations of compound **7c** (0.5, 1 and 2.5 μM) for 24 h, cells were collected by trypsinisation. The collected cells were washed twice with ice-cold PBS, then incubated with 200 μL 1 x binding buffer containing 5 μL Annexin V-FITC, and then in 300 μL 1 x binding buffer containing 5 μL Propidium iodide (PI) for 5 min at room temp in the dark. After 15 min of incubation, cells were analyzed for apoptosis using BD-c6 accuri flow-cytometer.

4.3.7. Quantikine ELISA Human Galectin-1 Immunoassay

This assay employs the quantitative sandwich enzyme immunoassay technique. A polyclonal antibody specific for human Galectin-1 has precoated on a microplate. Standards

and samples are pipetted into the wells and galectin-1 present is bound by the immobilized antibody. After washing away any unbound substances, an enzyme-linked polyclonal antibody specific for human Galectin-1 is added to the wells. The galectin levels were measured by using R & D human galectins quantikine ELISA kit (R & D Systems, USA).

4.3.8. Molecular modelling studies

The gal-1 was downloaded from PDB (PDB ID: 4Y24) for protein preparation wizard, and ready for docking i.e. removing water molecules, addition of missing side chains and, energy minimization by OPLS-2005 force field. The final compound **7c** was sketched using chemdraw, and converted to 3D using Ligprep. The Glide XP docking algorithm was utilized using a grid box volume of 10x 10x 10 Å at the centre of TD-139 as standard.

Acknowledgements

Department of Biotechnology (DBT), Govt. of India, New Delhi, for the young investigators in cancer biology start up grants (6242-19/RGCB/PMD/DBT /MLKA/2015).

Conflicts of Interest

Authors declared no conflicts

References

- [1] R.L. Siegel, K.D. Miller, A. Jemal, Cancer statistics, 2019, CA: A Cancer Journal for Clinicians. 69 (2019) 7–34.
- [2] F. Bray, J. Ferlay, I. Soerjomataram, R.L. Siegel, L.A. Torre, A. Jemal, Global cancer statistics 2018: GLOBOCAN estimates of incidence and mortality worldwide for 36 cancers in 185 countries, CA: A Cancer Journal for Clinicians. 68 (2018) 394–424.
- [3] R.L. Siegel, K.D. Miller, A. Jemal, Cancer statistics, 2020, CA: A Cancer Journal for Clinicians. 70 (2020) 7–30.
- [4] I. Camby, M. Le Mercier, F. Lefranc, R. Kiss, Galectin-1: a small protein with major functions, Glycobiology. 16 (2006) 137R-157R.
- [5] A. Paz, R. Haklai, G. Elad-Sfadia, E. Ballan, Y. Kloog, Galectin-1 binds oncogenic H-Ras to mediate Ras membrane anchorage and cell transformation, Oncogene. 20 (2001) 7486–7493.
- [6] C.B. Mello, L. Ramos, A.D. Gimenes, T.R. d. M. Andrade, S.M. Oliani, C.D. Gil, Immunomodulatory Effects of Galectin-1 on an IgE-Mediated Allergic Conjunctivitis Model, Investigative Ophthalmology & Visual Science. 56 (2015) 693–704.
- [7] G.A. Rabinovich, Galectin-1 as a potential cancer target, British Journal of Cancer. 92 (2005) 1188–1192.

- [8] L. Astorgues-Xerri, M.E. Riveiro, A. Tijeras-Raballand, M. Serova, C. Neuzillet, S. Albert, E. Raymond, S. Faivre, Unraveling galectin-1 as a novel therapeutic target for cancer, *Cancer Treatment Reviews*. 40 (2014) 307–319.
- [9] N. Martinez-Bosch, L.E. Barranco, C.A. Orozco, M. Moreno, L. Visa, M. Iglesias, L. Oldfield, J.P. Neoptolemos, W. Greenhalf, J. Earl, A. Carrato, E. Costello, P. Navarro, Increased plasma levels of galectin-1 in pancreatic cancer: potential use as biomarker, *Oncotarget*. 9 (2018).
- [10] Y.-L. Hsu, C.-Y. Wu, J.-Y. Hung, Y.-S. Lin, M.-S. Huang, P.-L. Kuo, Galectin-1 promotes lung cancer tumor metastasis by potentiating integrin $\alpha 6\beta 4$ and Notch1/Jagged2 signaling pathway, *Carcinogenesis*. 34 (2013) 1370–1381.
- [11] M.M. Alauddin, Positron emission tomography (PET) imaging with (18)F-based radiotracers, *Am J Nucl Med Mol Imaging*. 2 (2012) 55–76.
- [12] S. Vallabhajosula, (18)F-labeled positron emission tomographic radiopharmaceuticals in oncology: an overview of radiochemistry and mechanisms of tumor localization, *Semin Nucl Med*. 37 (2007) 400–419.
- [13] N.S. Goud, R.K. Joshi, R.D. Bharath, P. Kumar, Fluorine-18: A radionuclide with diverse range of radiochemistry and synthesis strategies for target based PET diagnosis, *European Journal of Medicinal Chemistry*. 187 (2020) 111979.
- [14] A. Singnurkar, R. Poon, U. Metser, Comparison of 18F-FDG-PET/CT and 18F-FDG-PET/MR imaging in oncology: a systematic review, *Annals of Nuclear Medicine*. 31 (2017) 366–378.
- [15] K.A. Kurdziel, J.D. Kalen, J.I. Hirsch, J.D. Wilson, R. Agarwal, D. Barrett, H.D. Bear, J.F. McCumiskey, Imaging multidrug resistance with 4-[18F]fluoropaclitaxel, *Nuclear Medicine and Biology*. 34 (2007) 823–831.
- [16] O. Shamni, H. Grievink, B. Itamar, E. Mishani, G. Abourbeh, Development of a Fluorinated Analogue of Erlotinib for PET Imaging of EGFR Mutation–Positive NSCLC, *Molecular Imaging and Biology*. 21 (2019) 696–704.
- [17] H. Su, Y. Seimbille, G.Z. Ferl, C. Bodenstein, B. Fueger, K.J. Kim, Y.-T. Hsu, S.M. Dubinett, M.E. Phelps, J. Czernin, W.A. Weber, Evaluation of [18F]gefitinib as a molecular imaging probe for the assessment of the epidermal growth factor receptor status in malignant tumors, *European Journal of Nuclear Medicine and Molecular Imaging*. 35 (2008) 1089–1099.
- [18] P. Kumar, B. Singh, A. Ghai, P.P. Hazari, B.R. Mittal, A.K. Mishra, Development of a single vial kit formulation of [99mTc]-labeled doxorubicin for tumor imaging and treatment response assessment-preclinical evaluation and preliminary human results: [99mTc]-doxorubicin kit development for tumor imaging, *Journal of Labelled Compounds and Radiopharmaceuticals*. 58 (2015) 242–249.
- [19] Salahuddin, M. Shaharyar, A. Mazumder, Benzimidazoles: A biologically active compounds, *Arabian Journal of Chemistry*. 10 (2017) S157–S173.

- [20] S. Tahlan, S. Kumar, B. Narasimhan, Pharmacological significance of heterocyclic 1H-benzimidazole scaffolds: a review, *BMC Chemistry*. 13 (2019).
- [21] N. Sridhar Goud, P. Kumar, R. Dawn Bharath, Recent Developments of Target-Based Benzimidazole Derivatives as Potential Anticancer Agents, in: *Heterocycles - Synthesis and Biological Activities*, IntechOpen, 2020.
- [22] Y. Bansal, O. Silakari, The therapeutic journey of benzimidazoles: A review, *Bioorganic & Medicinal Chemistry*. 20 (2012) 6208–6236.
- [23] K.P. Barot, S. Nikolova, I. Ivanov, M.D. Ghate, Novel research strategies of benzimidazole derivatives: a review, *Mini Rev Med Chem*. 13 (2013) 1421–1447.
- [24] G. Yadav, S. Ganguly, Structure activity relationship (SAR) study of benzimidazole scaffold for different biological activities: A mini-review, *European Journal of Medicinal Chemistry*. 97 (2015) 419–443.
- [25] T.-C. Shih, R. Liu, C.-T. Wu, X. Li, W. Xiao, X. Deng, S. Kiss, T. Wang, X.-J. Chen, R. Carney, H.-J. Kung, Y. Duan, P.M. Ghosh, K.S. Lam, Targeting Galectin-1 Impairs Castration-Resistant Prostate Cancer Progression and Invasion, *Clinical Cancer Research*. 24 (2018) 4319–4331.
- [26] T.-C. Shih, R. Liu, G. Fung, G. Bhardwaj, P.M. Ghosh, K.S. Lam, A Novel Galectin-1 Inhibitor Discovered through One-Bead Two-Compound Library Potentiates the Antitumor Effects of Paclitaxel *in vivo*, *Molecular Cancer Therapeutics*. 16 (2017) 1212–1223.
- [27] N.S. Goud, S.M. Ghose, J. Vishnu, D. Komal, V. Talla, R. Alvala, J. Pranay, J. Kumar, I.A. Qureshi, M. Alvala, Synthesis of 1-benzyl-1H-benzimidazoles as galectin-1 mediated anticancer agents, *Bioorganic Chemistry*. 89 (2019) 103016.
- [28] N.S. Goud, V. Pooladanda, G.S. Mahammad, P. Jakkula, S. Gatreddi, I.A. Qureshi, R. Alvala, C. Godugu, M. Alvala, Synthesis and biological evaluation of morpholines linked coumarin–triazole hybrids as anticancer agents, *Chemical Biology & Drug Design*. 94 (2019) 1919–1929.
- [29] T.G. Kraljević, A. Harej, M. Sedić, S.K. Pavelić, V. Stepanić, D. Drenjančević, J. Talapko, S. Raić-Malić, Synthesis, *in vitro* anticancer and antibacterial activities and *in silico* studies of new 4-substituted 1,2,3-triazole–coumarin hybrids, *European Journal of Medicinal Chemistry*. 124 (2016) 794–808.
- [30] D.N. Kommi, D. Kumar, R. Bansal, R. Chebolu, A.K. Chakraborti, “All-water” chemistry of tandem N-alkylation–reduction–condensation for synthesis of N-arylmethyl-2-substituted benzimidazoles, *Green Chemistry*. 14 (2012) 3329.
- [31] S.I. Alaqeel, Synthetic approaches to benzimidazoles from o-phenylenediamine: A literature review, *Journal of Saudi Chemical Society*. 21 (2017) 229–237.
- [32] F. Dollé, [18F]Fluoropyridines: From Conventional Radiotracers to the Labeling of Macromolecules Such as Proteins and Oligonucleotides, in: P.A. Schubiger, L. Lehmann, M. Friebe (Eds.), *PET Chemistry*, Springer Berlin Heidelberg, 2007: pp. 113–157.

- [33] D. Vaulina, M. Nasirzadeh, N. Gomzina, Automated radiosynthesis and purification of [¹⁸F]flumazenil with solid phase extraction, *Applied Radiation and Isotopes*. 135 (2018) 110–114.
- [34] M. Mihon, C. Tuta, R. Leonte, A.C. Ion, V. Lavric, D. Niculae, AN IMPROVED METHODOLOGY FOR DETERMINATION OF RADIOCHEMICAL AND CHEMICAL IMPURITIES IN THE SYNTHESIS PROCESS OF ¹⁸F-FDG (2-[¹⁸F] FLUORO-2-DEOXY-D-GLUCOSE), *Environmental Engineering and Management Journal*. 14 (2015) 289–296.
- [35] N.S. Goud, M.S. Ghose, J. Vishnu, J. Pranay, R. Alvala, V. Talla, I.A. Qureshi, M. Alvala, Synthesis and Biological Evaluation of Novel Heterocyclic Imines Linked Coumarin- Thiazole Hybrids as Anticancer Agents, *Anti-Cancer Agents in Medicinal Chemistry*. 19 (2019) 557–566.
- [36] N.S. Goud, V. Pooladanda, G.S. Mahammad, P. Jakkula, S. Gatreddi, I.A. Qureshi, R. Alvala, C. Godugu, M. Alvala, Synthesis and biological evaluation of morpholines linked coumarin–triazole hybrids as anticancer agents, *Chemical Biology & Drug Design*. 94 (2019) 1919–1929.
- [37] A.K. Estandarte, S. Botchway, C. Lynch, M. Yusuf, I. Robinson, The use of DAPI fluorescence lifetime imaging for investigating chromatin condensation in human chromosomes, *Scientific Reports*. 6 (2016).
- [38] S. Narva, S. Chitti, S. Amaroju, S. Goud, M. Alvala, D. Bhattacharjee, N. Jain, C.S. Kondapalli Venkata Gowri, Design, Synthesis, and Biological Evaluation of 2-(4-Aminophenyl)benzothiazole Analogues as Antiproliferative Agents: Design, Synthesis, and Biological Evaluation of 2-(4-Aminophenyl)benzothiazole Analogues as Antiproliferative Agents, *Journal of Heterocyclic Chemistry*. 56 (2019) 520–532.
- [39] N.S. Goud, V.K. Kanth Makani, J. Pranay, R. Alvala, I.A. Qureshi, P. Kumar, R.D. Bharath, C. Nagaraj, S. Yerramsetty, M. Pal-Bhadra, M. Alvala, Synthesis, ¹⁸F-radiolabeling and apoptosis inducing studies of novel 4, 7-disubstituted coumarins, *Bioorganic Chemistry*. 97 (2020) 103663.
- [40] A.M. Rieger, K.L. Nelson, J.D. Konowalchuk, D.R. Barreda, Modified Annexin V/Propidium Iodide Apoptosis Assay For Accurate Assessment of Cell Death, *Journal of Visualized Experiments*. (2011).
- [41] N.S. Goud, P.S.L. Soukya, M. Ghose, D. Komal, R. Alvala, M. Alvala, Human Galectin-1 and Its Inhibitors: Privileged Target for Cancer and HIV, *Mini-Reviews in Medicinal Chemistry*. 19 (2019) 1369–1378.
- [42] N.S. Goud, P. Kumar, R.D. Bharath, Recent Developments of Target based Coumarin Derivatives as Potential Anticancer Agents, *Mini-Reviews in Medicinal Chemistry*. 20 (2020).
- [43] R. Méjard, B. Thierry, Systematic Study of the Surface Plasmon Resonance Signals Generated by Cells for Sensors with Different Characteristic Lengths, *PLoS ONE*. 9 (2014) e107978.

[44] P. Khadkikar, N.S. Goud, A. Mohammed, G. Ramamoorthy, R. Ananthathatmula, M. Doble, A. Rizvi, S. Banerjee, A. Ravi, M. Alvala, An efficient and facile green synthesis of bisindole methanes as potential *Mtb* FtsZ inhibitors, *Chemical Biology & Drug Design*. 92 (2018) 1933–1939.

[45] K. Daipule, N.S. Goud, A. Sethi, S. Gurrapu, E. Mamidala, M. Alvala, Synthesis, molecular docking simulation, and biological evaluation studies of novel amide and ether conjugates of 2,3-diaryl-1,3-thiazolidin-4-ones, *Journal of Heterocyclic Chemistry*. 57 (2020) 774–790.

Journal Pre-proofs

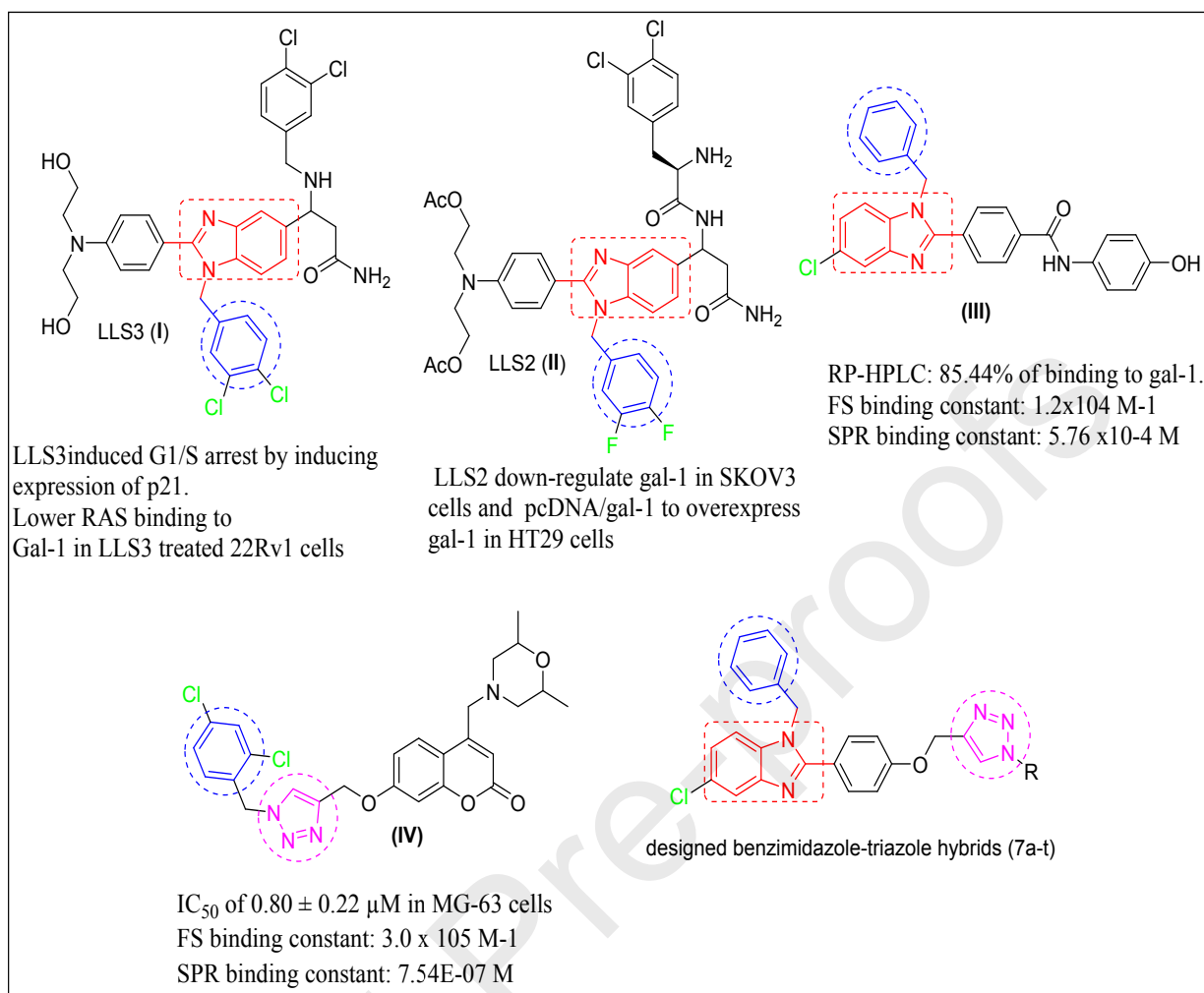


Figure 1. Representative examples of available benzimidazole-triazole derivatives, and rationale for the designed target compounds 7a-t.

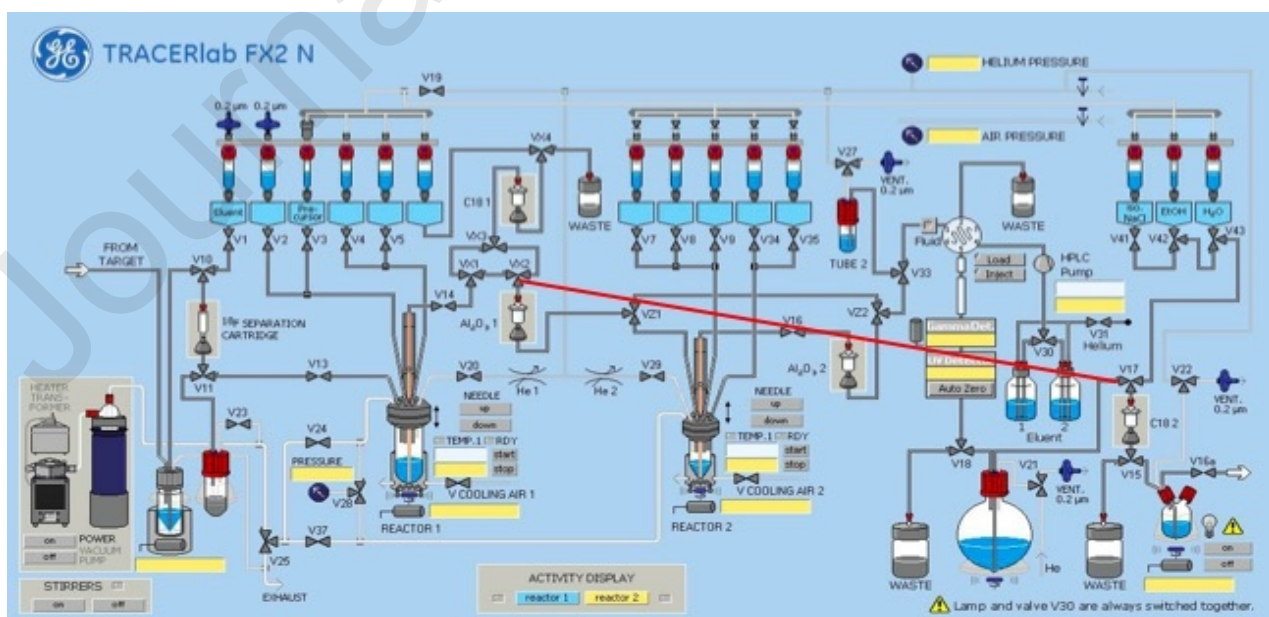


Figure 2. Schematic view of the modified GE Tracer-lab FX2N module (automated synthesizer) through the direct connection from the left output of VX2 to the V17.

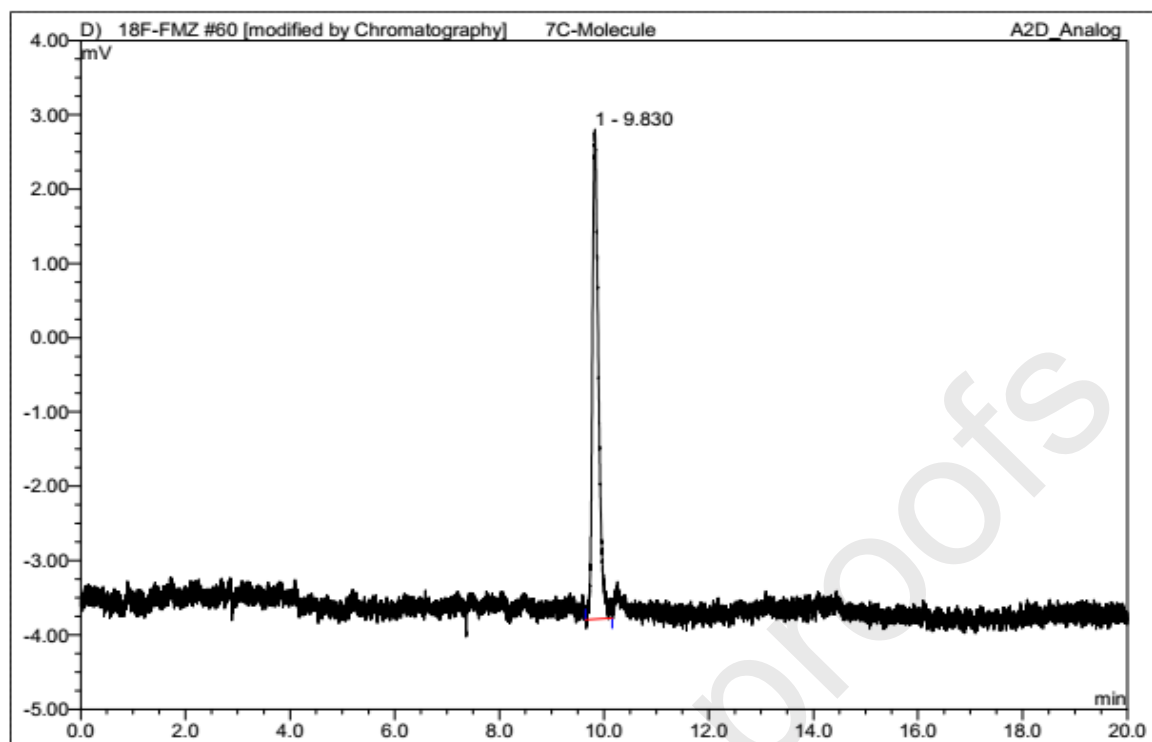


Figure 3A. Typical HPLC chromatogram of ^{18}F -7c, detected by radio-detector.

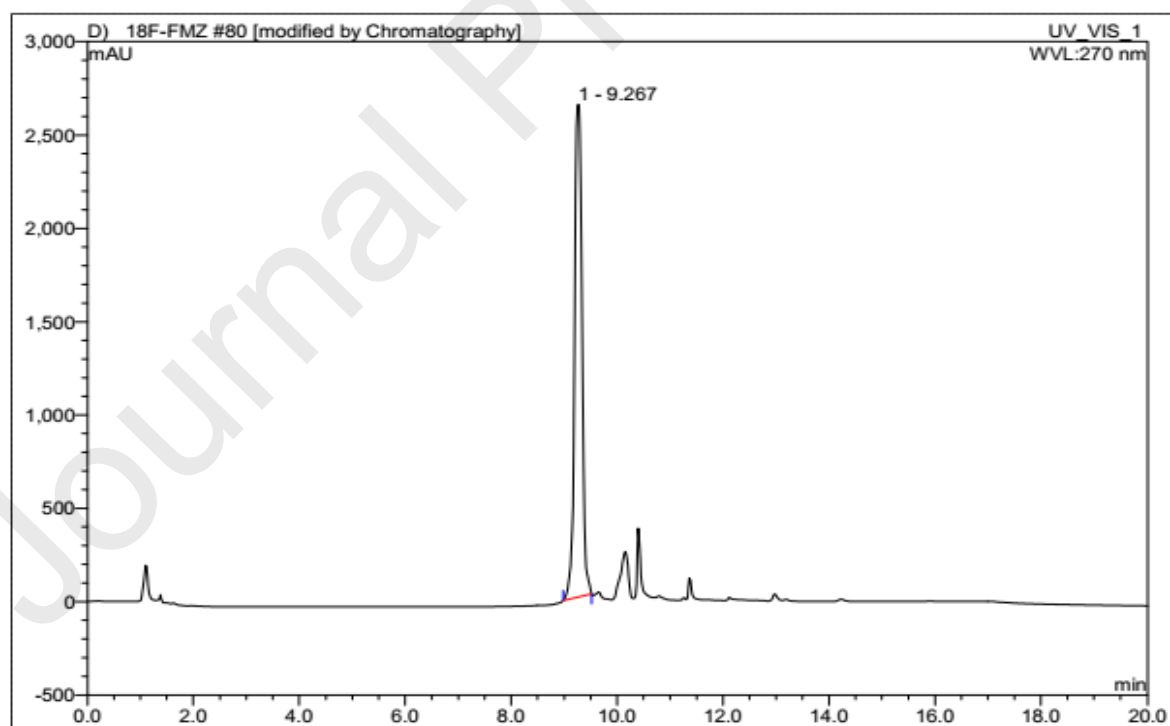


Figure 3B. Typical HPLC chromatogram of the cold compound 7c, detected by UV-detector at 270 nm.

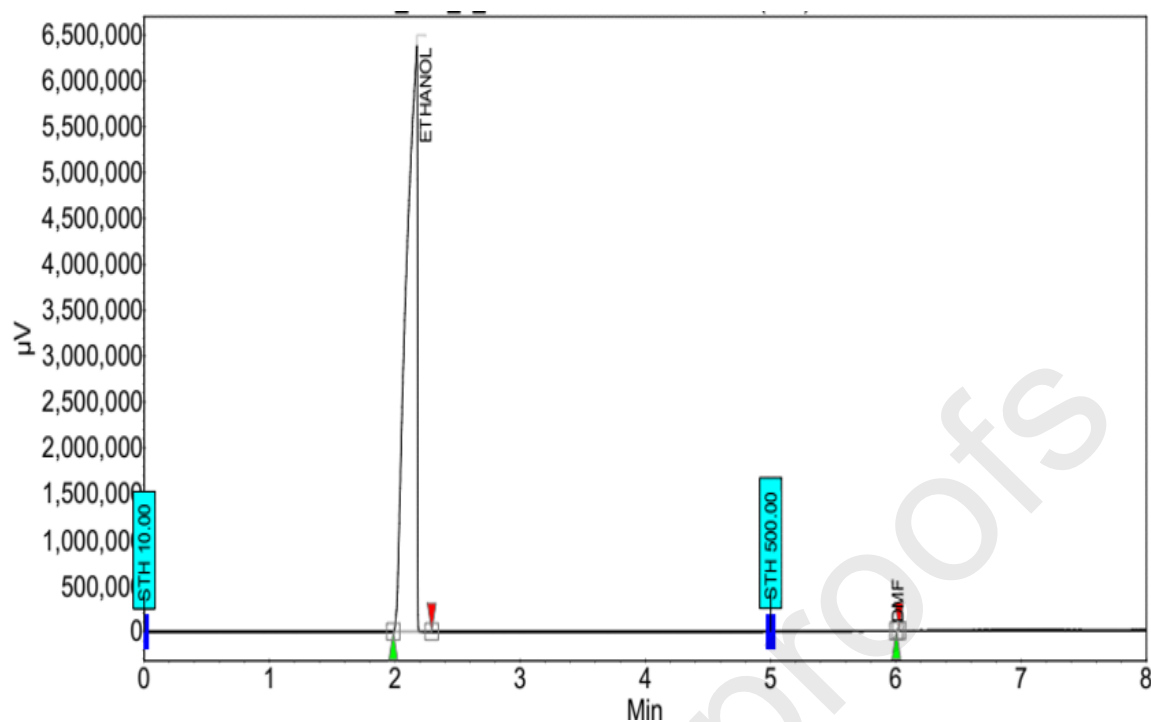


Figure 4. The GC results of ^{18}F -7c compound and showed the peaks of ethanol and DMF in ppm levels.

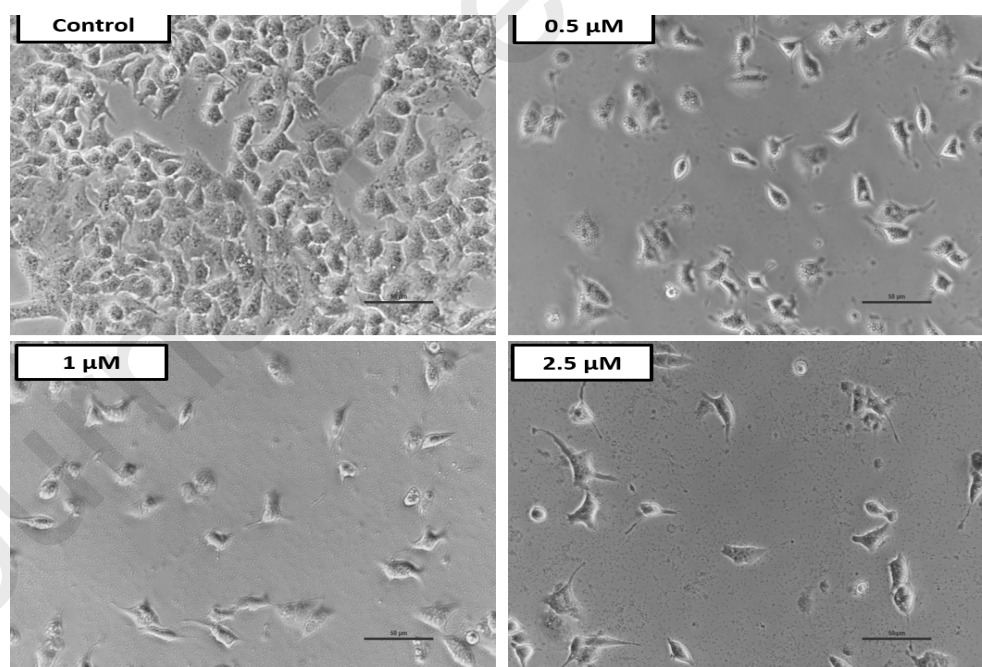


Figure 5. Morphological changes due to induction of apoptosis by 7c were observed by phase-contrast microscopy. The A-549 cells lost their characteristics of epithelial cells with increasing concentrations of 7c.

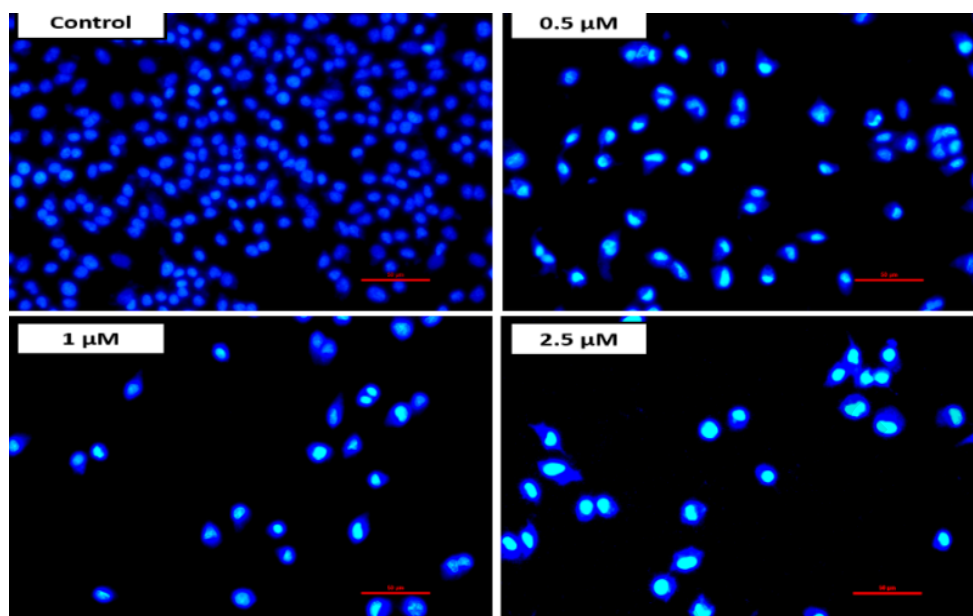


Fig. 6. Nuclear morphology of A-549 cells treated with **7c**: Nuclear morphology of A-549 cancer cells visualised after DAPI staining. cells were treated with different concentrations of **7c** compound for 48 h and stained with DAPI. The images were captured with fluorescence microscope at 200X.

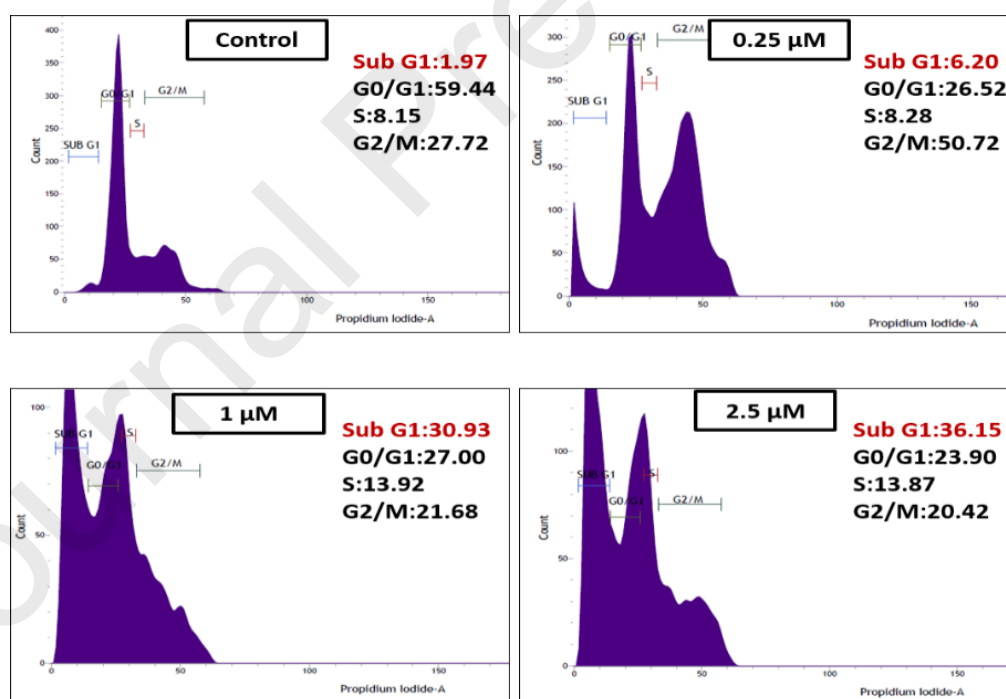


Figure 7. Cell cycle analysis: A-549 Cells were treated with 0.25, 1 and 2.5 μ M concentrations **7c** and analysed by propidium iodide (PI) staining after 24 h of incubation.

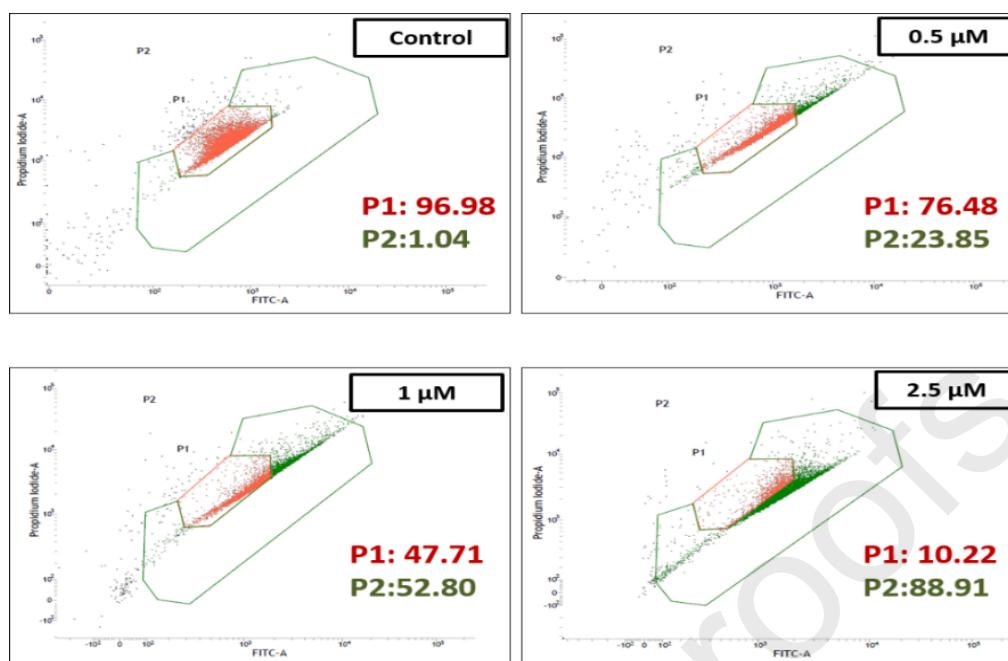


Figure 8. Flowcytometric analysis of the mitochondrial membrane potential: mitochondrial membrane depolarisation of A-549 cells treated with 0.5, 1 and 2.5 μ M concentrations of **7c**. P1(red) indicates the percentage of polarised cells (live), where is P2(green) indicates the percentage of depolarised cells (dead).

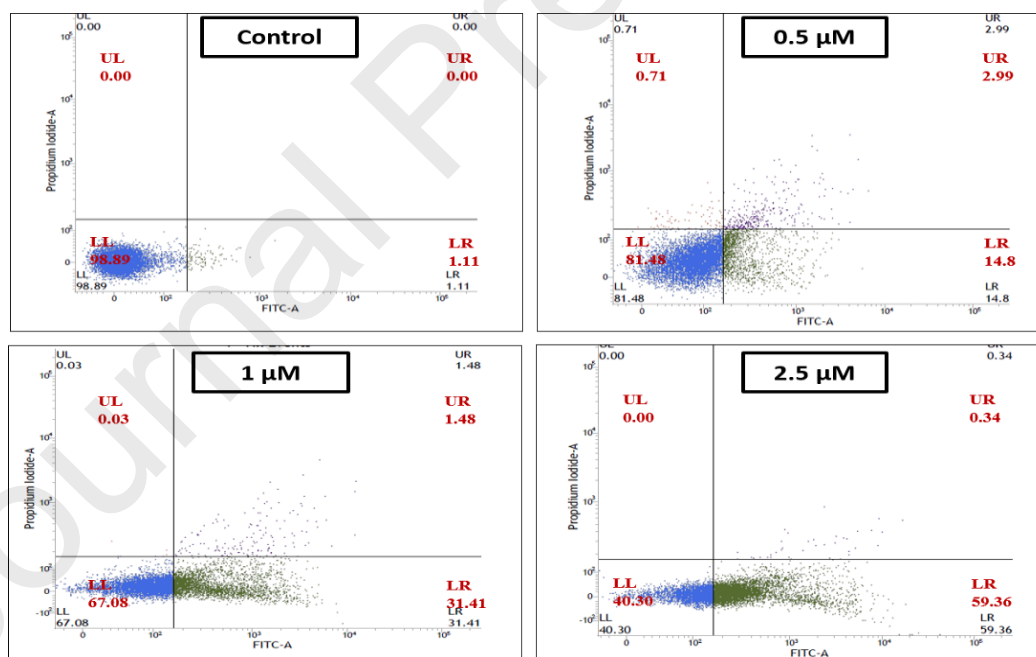


Figure 9. Effect of compound **7c** on induction of apoptosis in A-549 cells. After 48 h of compound **7c** (0.5, 1 and 2.5 μ M) incubation, cells were stained with Annexin V/PI and analysed for apoptosis using BD c6 accuri flow cytometer. 59.36% apoptotic cells were observed at 2.5 μ M concentration. The 10,000 cells from each sample were analysed by flow cytometry.

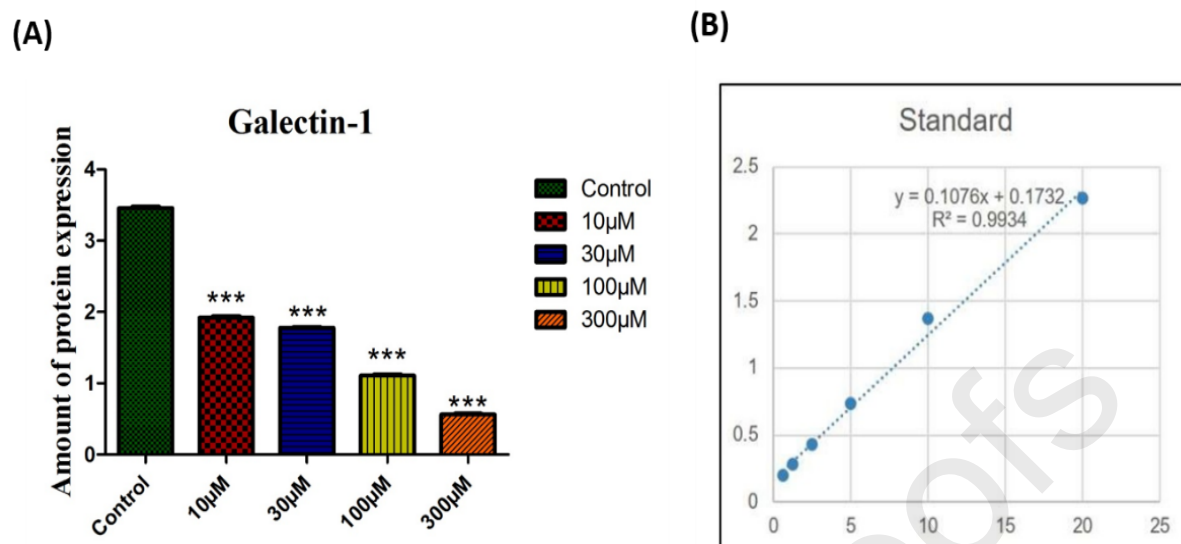


Figure 10. (A) Gal-1 protein levels in A-549 cells with or without **7c** at 10, 30, 100 and 300 μM concentration. (B) Human Gal-1 Standard Curve. (Data represent as Mean \pm SEM, *** $p < 0.001$, **7c** vs. control).

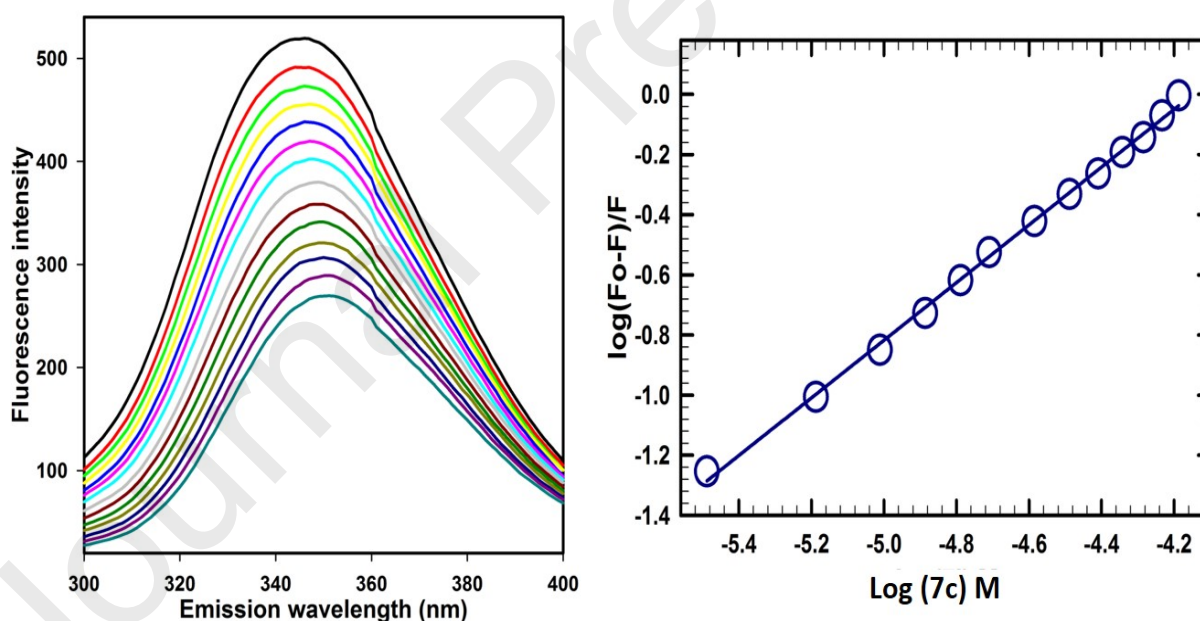


Figure 11. Fluorescence binding study of compound **7c** with the Gal-1. (A) Fluorescence spectra of Gal-1 in the increasing concentrations of ligand from 0 to 65 μM (from top to bottom) at pH 7.5. The protein was excited at 280 nm and emission spectra was collected in the range of 300–400 nm. (B) Modified Stern–Volmer plot of Gal-1 by compound **7c** used for the calculation of binding affinity.

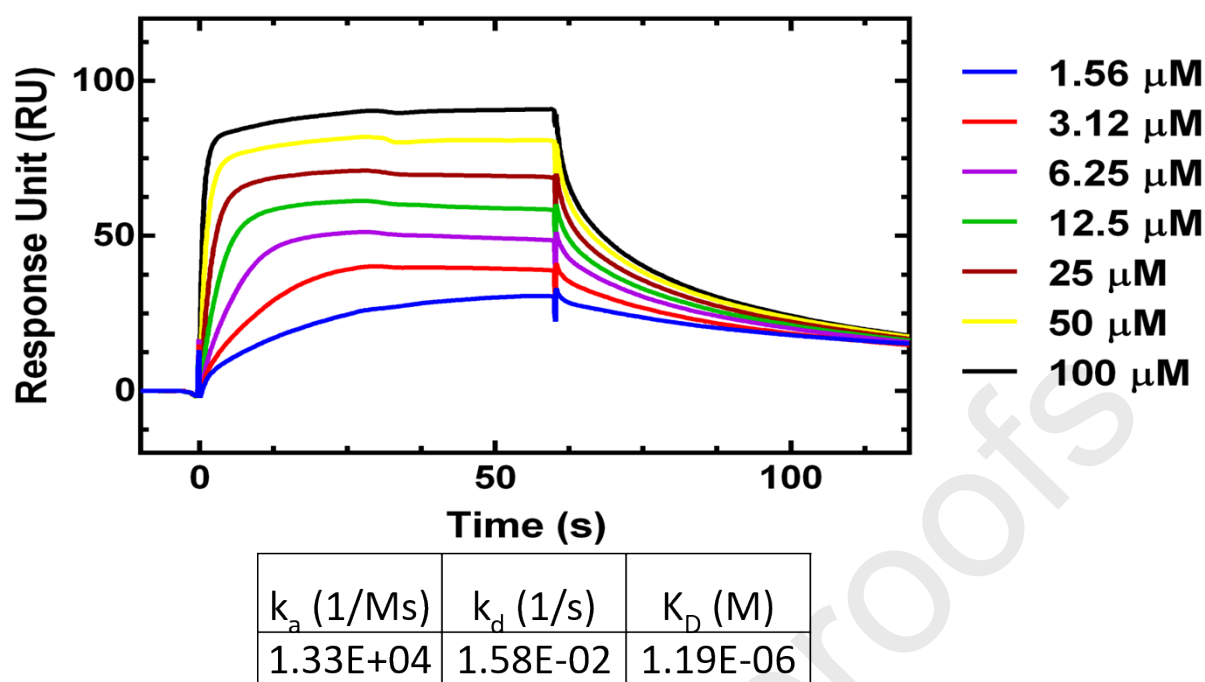


Figure 12. Sensorgram of SPR for Gal-1 binding to compound **7c**. The y-axis represents the amount of bound analyte in terms of RU, while x-axis shows time after injection (seconds). The colored lines indicate different concentrations of compound **7c** viz. 200 μ M (Red), 100 μ M (Green), 50 μ M (Blue), 25 μ M (Black) and 12.5 μ M (Purple).

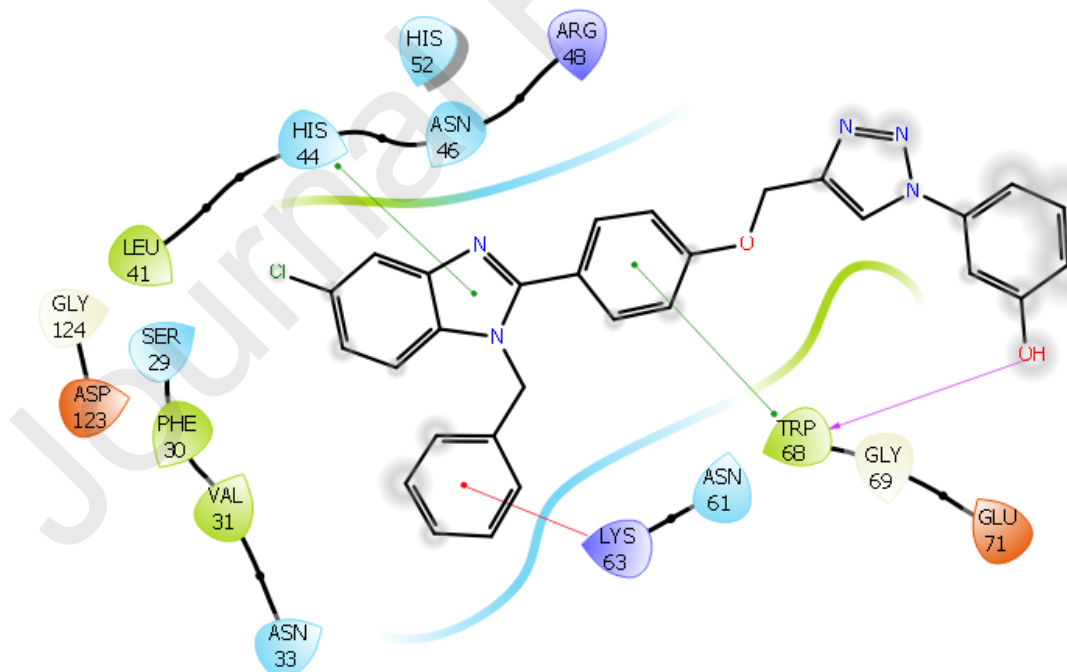


Figure 13A: 2D ligand interaction diagram of compound **7c** with the active site of Gal-1 protein (PDB ID: 4Y24).

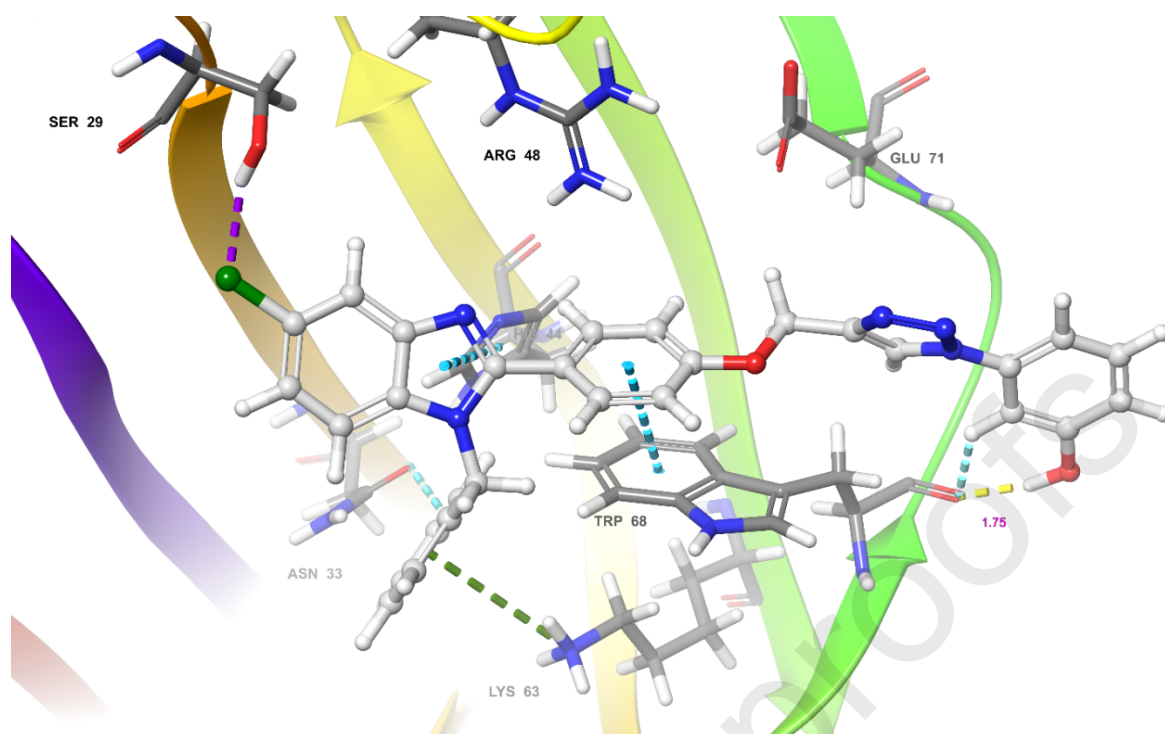


Figure 13A: 3D ligand interaction diagram of compound **7c** with the active site of Gal-1 protein (PDB ID: 4Y24).

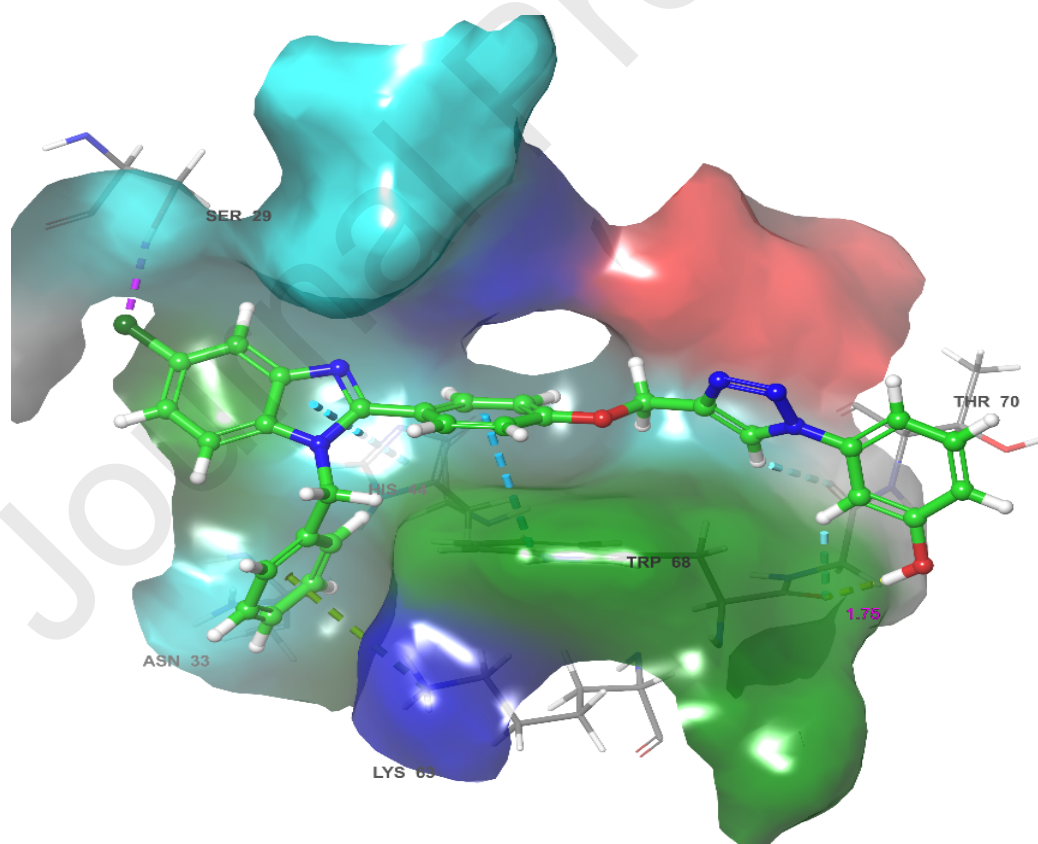
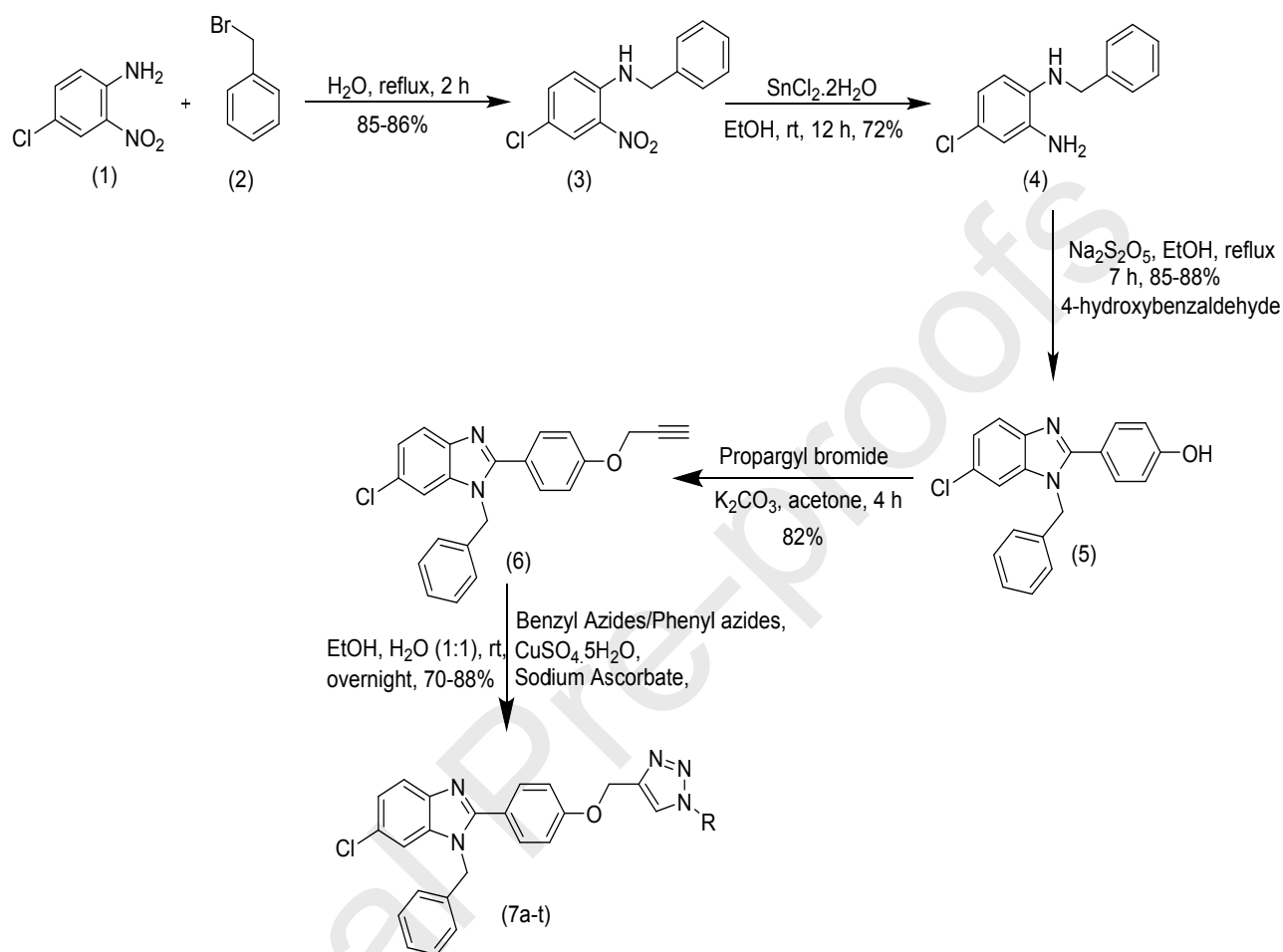


Figure 13C: 3D surface energy diagram of compound **7c** with the active site of Gal-1 protein (PDB ID: 4Y24).

Scheme-1



7a R = Phenyl-

7b R = 2-methoxy Phenyl-

7c R = 3-hydroxy Phenyl-

7d R = 4--methyl Phenyl-

7e R = 4-trifluoro Phenyl-

7f R = 4-fluoro Phenyl-

7g R = 3-fluoro Phenyl-

7h R = 4-bromo Phenyl-

7i R = 4-nitro-2-Chloro Phenyl-

7j R = 3-nitro-4-methyl Phenyl-

7k R = 3-nitro Phenyl-

7l R = benzyl-

7m R = 2-nitro benzyl-

7n R = 4-nitro benzyl-

7o R = 2-fluoro benzyl -

7p R = 3,5-difluoro benzyl-

7q R = 4-bromo benzyl-

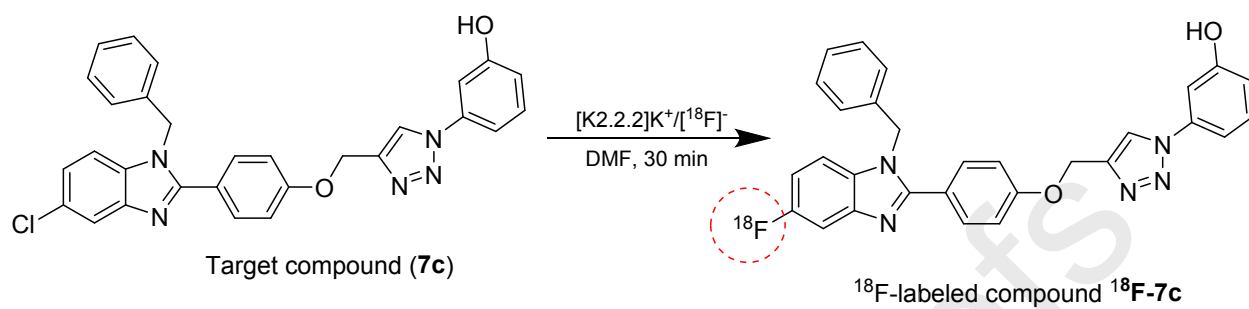
7r R = 2-bromo benzyl-

7s R = 2,3-dimethyl Phenyl-

7t R = naphthyl-

Scheme 1. Synthesis of different benzimidazole-triazole analogues **7a-t**.

Scheme-2



Scheme 2. Radiolabeling of target molecule **7c** with ¹⁸F radionuclide *via aromatic nucleophilic* radio-fluorination.

Table 1. IC₅₀ (μM) values^a for the derivatives **7a-t** by MTT assay.

Compound	MCF-7 ^b	NCI-H460 ^c	MDA-MB-231 ^d	A-549 ^e	HaCaT ^f
7a	>15	>15	>15	>15	>15
7b	6.53±0.12	2.08±0.04	2.42±0.04	1.71±0.21	4.96±2.71
7c	1.3±0.18	0.99±0.01	0.94±0.02	0.63±0.21	2.99±0.09
7d	>15	>15	>15	>15	>15
7e	>15	>15	>15	>15	>15
7f	1.21±0.17	3.93±0.07	1.78±0.18	2.14±0.08	3.31±0.01
7g	4.07±0.17	8.58±0.28	2.37±0.24	1.11±0.12	5.94±0.06
7h	>15	>15	>15	>15	>15
7i	1.62±0.02	3.41±0.16	1.65±0.05	1.87±0.06	3.08±0.11
7j	>15	>15	>15	>15	>15
7k	>15	>15	>15	>15	>15
7l	>15	>15	>15	>15	>15
7m	>15	>15	>15	>15	>15
7n	1.31±0.1	1.98±0.08	2.63±0.11	4.52±0.16	1.35±0.09
7o	>15	>15	>15	>15	>15
7p	>15	>15	>15	>15	>15
7q	>15	>15	>15	>15	>15
7r	>15	>15	>15	>15	>15
5-fluorouracil	2.80 ±0.12	3.20 ± 0.50	0.79 ±0.09	1.69 ±0.90	1.16 ± 0.06

^a50% Inhibitory concentration after 48 h of drug treatment. ^{b, d} Human breast cancer. ^{c, e} Human lung cancer. ^f Human keratinocyte cancer.

Table 2. Amount of Gal-1 protein in control and compound **7c** (10, 30, 100 and 300 μM) treated A-549 cells.

Concentration	Absorbance at 450 nm	Gal-1 concentration(μg/mL)
Control	0.5453	3.45
7c (10 μM)	0.3800	1.92
7c (30 μM)	0.3645	1.77
7c (100 μM)	0.2926	1.10
7c (300 μM)	0.2337	0.56

Table 3: The physicochemical properties (ADMET) of **compound 7c** were calculated using *qikprop* program are listed below.

S. No	Properties or Descriptors	Recommended Values	Compound 7q
1	Molecular weight	130.0 – 725.0	507.978
2	Dipole moment	1.0 – 12.5	10.503
3	Total SASA	300.0 – 1000.0	850.856
4	Molecular Volume	500.0 – 2000.0	1531.299
5	No. of rotatable bonds	0 – 15	6
6	Donor HB	0.0 – 6.0	1
7	Acceptor HB	2.0 – 20.0	5
8	QP Polarizability	13.0 – 70.0	56.941
9	QP logP o/w	2.0 – 6.5	6.896
10	QP log BB	-3.0 – 1.2	-1.112
11	QP log HERG	Concern below -5	-8.323
12	Human Oral Absorption	1-3	1
13	Percent Human Oral Absorption	>80% is high	91.312
14	Rule of Five violations	<25% is low	2
15	No. of metabolites	Maximum of 4	4

Novel Benzimidazole-Triazole Hybrids as Apoptosis Inducing Agents in Lung Cancer: Design, Synthesis, ^{18}F -Radiolabeling & Galectin-1 Inhibition Studies.

Nerella Sridhar Goud ^{a, b}, Venkatesh Pooladanda ^c, Muni Chandra K ^a, **P.S. Lakshmi Soukya** ^a, Ravi Alvala ^d, Pardeep Kumar ^b, Chandana Nagraj ^b, Rose Dawn Bharath ^b, Insaf A. Qureshi ^e, Chandraiah Godugu ^c, Mallika Alvala ^{a*}

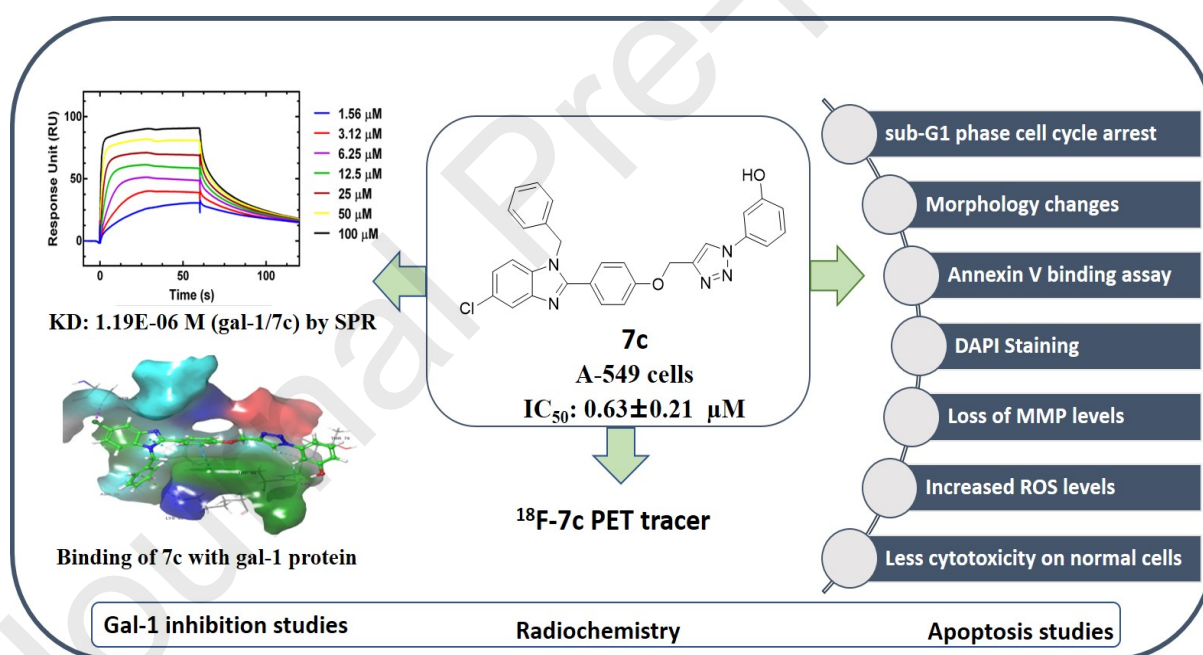
^a Department of Medicinal Chemistry, National Institute of Pharmaceutical Education and Research (NIPER), Hyderabad 500 03 7, India

^b Department of Neuroimaging and Interventional Radiology (NI & IR), National Institute of Mental Health and Neuro Sciences (NIMHANS), Bangalore 560 029, India.

^c Department of Regulatory Toxicology, National Institute of Pharmaceutical Education and Research (NIPER), Hyderabad 500 037, India

^d G. Pulla reddy College of Pharmacy (GPRCP), Hyderabad 500 028, India

^e Department of Biotechnology & Bioinformatics, School of Life Sciences, University of Hyderabad (UOH), Hyderabad-500046, India.



Research Highlights

- The **7c** is a potent cytotoxic agent against global major leading lung cancer burden.
- It has shown IC_{50} of 0.63 ± 0.21 μ M, and 0.99 ± 0.01 μ M in lung cancer cells (A-549 and NCI-H460) mediated by gal-1.
- The **7c** is capable of binding with gal-1 based on the confirmation studies of SPR, and FS.
- The ^{18}F -**7c** radiotracer is considered as an ideal PET tracer due to its 110 min half-life.
- The radiochemical purity & identity of ^{18}F -**7c** was validated as per **cGMP guidelines for clinical evaluation.**

Declaration of interests

The authors declare that they have no known competing financial interests or personal relationships that could have appeared to influence the work reported in this paper.

The authors declare the following financial interests/personal relationships which may be considered as potential competing interests:

Nil